Chronology and processes of late Quaternary hillslope sedimentation in the eastern South Island, New Zealand

Borella, Josh; Quigley, Mark; Sohbati, Reza; Almond, Peter; Gravley, Darren M.; Murray, Andrew Sean

Published in:
Journal of Quaternary Science

Link to article, DOI:
10.1002/jqs.2905

Publication date:
2016

Document Version
Peer reviewed version

Journal of Quaternary Science

Stratigraphy and chronology of late Quaternary loessic hillslope sediments reveals seismic, climatic, and anthropogenic influences on surface processes, eastern South Island, New Zealand

Journal:	*Journal of Quaternary Science*
Manuscript ID	JQS-16-0031
Wiley - Manuscript type:	Research Article
Date Submitted by the Author:	12-Mar-2016
Complete List of Authors:	Borella, Josh; University of Canterbury, Geological Sciences; Quigley, Mark ; University of Melbourne, School of Earth Sciences Sohbati, Reza; Danmarks Tekniske Universitet Campus Risoe, Nutech; Aarhus Universitet, Nordic Laboratory for Luminescence Dating, Department of Geoscience Kuklewicz, Katherine; University of Kansas, Department of Geology Murray, Andrew; Aarhus Universitet, Nordic Laboratory for Luminescence Dating, Department of Geoscience Gravley, Darren; University of Canterbury, Geological Sciences
Keywords:	rockfall, paleoseismicity, hillslope response, OSL, radiocarbon

Stratigraphy and chronology of late Quaternary loessic hillslope sediments reveals seismic, climatic, and anthropogenic influences on surface processes, eastern South Island, New Zealand

Corresponding Author:

Josh Borella
Department of Geological Sciences
University of Canterbury, New Zealand

Email: *josh.borella@pg.canterbury.ac.nz*

Abstract

Optical and radiocarbon dating of loessic hillslope sediments in New Zealand's South Island is used to constrain the timing of prehistoric rockfalls and associated seismic events, quantify spatial and temporal patterns of landscape evolution, and examine hillslope responses to climatic and anthropogenic forcing. Exploratory trenches adjacent to prehistoric boulders enable stratigraphic analysis of loess and loess-colluvium pre- and post-boulder emplacement sediments. Luminescence ages from colluvial sediments constrain timing of boulder emplacement to between ~3.0 and ~12.5 ka, well before the arrival of Polynesians (c. AD 1280) and Europeans (c. AD 1800) in New Zealand. Three phases of colluviation are revealed at the Rapaki study site, reflecting natural and anthropogenic-driven shifts in sedimentation and landscape evolution. Sediment accumulation rates increased considerably (>15 factor increase) following human arrival and associated anthropogenic burning of hillslope vegetation. Phytolith results suggest paleo-vegetation at Rapaki was compositionally variable and persisted under a predominantly cool temperature environment with warm-temperate elements. Palm phytolith abundances imply maximum climate warming during early (~12-11 ka) and late (~3-2 ka) Holocene phases. This study provides insights into the spatial and temporal patterns of hillslope evolution, highlighting the roles of climate change, earthquakes, and humans on surface processes.

Keywords: rockfall, paleoseismicity, hillslope response, OSL, radiocarbon

Stratigraphy and chronology of late Quaternary loessic hillslope sediments reveals seismic, climatic, and anthropogenic influences on surface processes, eastern South Island, New Zealand

Authors: Josh Borella[1*], Mark Quigley[2], Reza Sohbati[3,5], Katherine Kuklewicz[4], Andrew Murray[5], Darren Gravley[1]

[1]Department of Geological Sciences, University of Canterbury, New Zealand
[2]School of Earth Sciences, The University of Melbourne, Victoria 3010, Australia
[3]Technical University of Denmark, Centre for Nuclear Technologies, DTU-Nutech, DTU Riso Campus, DK-4000, Roskilde, Denmark
[4]Department of Geology, University of Kansas, Kansas 66045, USA
[5]Nordic Laboratory for Luminescence Dating. Department of Geoscience, Aarhus University, DTU Riso Campus, DK-4000, Roskilde, Denmark

*Corresponding author: josh.borella@pg.canterbury.ac.nz

Abstract

Optical and radiocarbon dating of loessic hillslope sediments in New Zealand's South Island is used to constrain the timing of prehistoric rockfalls and associated seismic events, quantify spatial and temporal patterns of landscape evolution, and examine hillslope responses to climatic and anthropogenic forcing. Exploratory trenches adjacent to prehistoric boulders enable stratigraphic analysis of loess and loess-colluvium pre- and post-boulder emplacement sediments. Luminescence ages from colluvial sediments constrain timing of boulder emplacement to between ~3.0 and ~12.5 ka, well before the arrival of Polynesians (c. AD 1280) and Europeans (c. AD 1800) in New Zealand. Three phases of colluviation are revealed at the Rapaki study site, reflecting natural and anthropogenic-driven shifts in sedimentation and landscape evolution. Sediment accumulation rates increased considerably (>15 factor increase) following human arrival and associated anthropogenic burning of hillslope vegetation. Phytolith results suggest paleo-vegetation at Rapaki was compositionally variable and persisted under a predominantly cool temperature environment with warm-temperate elements. Palm phytolith abundances imply maximum climate warming during early (~12-11 ka) and late (~3-2 ka) Holocene phases. This study provides insights into the spatial and temporal

patterns of hillslope evolution, highlighting the roles of climate change, earthquakes, and humans on surface processes.

1. Introduction

Hillslope sediments provide a potentially valuable archive of contemporary and paleo-landscape processes (e.g. Fuchs and Lang, 2009; Fuchs et al., 2010). Dating of slope sediments has been extensively used for understanding landscape response to local and global climate change (e.g. Hanson et al., 2004), anthropogenic influences on hillslope sediment erosion and accumulation (e.g. Fuchs et al., 2004, 2010; Almond et al., 2008), and tectonic activity (e.g. Fattahi et al., 2006). Additionally, hillslope sediment chronologies have been used to determine the timing of mass wasting events, such as landslides and rockfalls (e.g. Chapot et al., 2012; Matmon et al., 2005; Mackey and Quigley, 2014; Rinat et al., 2014; Sohbati et al., in review).

Various methods have been used to date hillslope sediments (e.g. Lang et al., 1999), including radiocarbon dating (^{14}C) (e.g. Stout, 1969; Bertolini, 2007), lichenometry (e.g. Bull et al., 1994; Luckman and Fiske, 1995; Andre, 1997; McCarroll et al., 2001), dendrochronology (e.g. Stoffel, 2006), and optically stimulated luminescence (OSL) dating (e.g. Matmon et al., 2005; Balescu et al., 2007; Chapot et al., 2012; Sohbati et al., in review). Cosmogenic nuclide (CN) surface exposure dating has also been used to determine the emplacement time for boulders entrenched within hillslope sediments (e.g. Cordes et al., 2013; Mackey and Quigley, 2014; Rinat et al., 2014; Stock et al. 2014). Increased confidence in hillslope sediment chronologies can be obtained by combining OSL, ^{14}C and CN (e.g. Lang and Wagner, 1996, 1997); and when this is coupled with the study of complimentary paleo-vegetation and paleo-climate indicators (e.g. phytoliths, pollen), important information about climatic, seismogenic, and anthropogenic activities and their influence on landscape evolution may be obtained (e.g. McWethy et al., 2010).

New Zealand's South Island provides a variety of important opportunities for investigating the spatiotemporal behavior of surface processes and their response to

seismic, climatic, and anthropogenic forcing (e.g. Almond et al., 2008; Hughes et al., 2010; Glade, 2003; Fuller et al., 2015; Rowan et al., 2012). In this paper we perform detailed analysis (e.g. stratigraphic logging, grain-size analysis, sediment bulk density, phytolith identification) and OSL and ^{14}C dating of loessic hillslope sediments to (1) constrain the timing of prehistoric rockfall and associated seismogenic events, (2) quantify spatial and temporal patterns of landscape evolution (including vegetation cover), and (3) examine hillslope responses to climatic and anthropogenic forcing. In combination with Sohbati et al. (in review) we present the first successful (i.e. reliable luminescence ages) optical dating of coarse-grained (i.e. >11 μm) loess and loess-colluvium hillslope sediments in New Zealand using the SAR protocol for quartz and $pIRIR_{290}$ protocol for K-rich feldspar. The results, along with Mackey and Quigley (2014) ^{3}He CN surface exposure ages, constrain timing of prehistoric rockfall events and provide insights into the spatial and temporal patterns of hillslope evolution, highlighting the roles of climate change, earthquakes, and humans on surface processes.

2. Geologic and Climatic Setting

2.1 Geology of Banks Peninsula and the Port Hills

Banks Peninsula (Fig. 1a) is comprised of three main volcanoes active between ~11.0 and 5.8 Ma (Hampton and Cole, 2009). The landscape is typified by deeply incised erosional valleys radiating outward from volcanic cone centers with bounding ridges of less eroded material. The study site is located within the dissected Lyttelton Volcanic complex (~11.0-9.7 Ma) on the western side of Banks Peninsula (Fig. 1a). Bedrock of the Lyttelton Volcanic complex is composed of subaerial basaltic and trachytic lava flows interlayered with ash and/or paleosol packages (Forsyth et al. 2008; Hampton and Cole, 2009). The volcanic rocks are mantled by four principal regolith materials: windblown loess, loess-colluvium, mixed loess-volcanic colluvium, and volcanic colluvium, as defined by Bell and Trangmar (1987)

The initiation and timing of regionally-sourced (Southern Alps and Canterbury Plains, see Fig. 1) windblown loess accumulation on Banks Peninsula has been the subject of previous studies at multiple locations (cf. Griffiths, 1973; Ives, 1973; Almond et al., 2007). Results from Almond et al. (2007) indicate the last major phase of loess accumulation on the lower flanks of Banks Peninsula in Canterbury began before ca 30,000 14C yr BP (ca. 35,000 cal. yr BP). They obtained a feldspar IRSL age of 17,300 ± 1,000 from near the top of the same sequence. Humic acid from the uppermost identified paleosol near the top of a section of correlative loessic units at another location yielded a ^{14}C age of 17,450 ± 2,070 cal. years B.P. (Griffiths, 1973).

Almond et al. (2008) investigated hillslope response at Ahuriri Quarry on the western flank of Banks Peninsula and conclude that most erosion occurred in the Holocene after the primary loess accumulation phase (~35-17 ka), consistent with an increase in soil flux rates with Holocene climate amelioration and recolonization by forest. Their results suggest a complex interaction between climate, vegetation, land management and soil transport on soil mantled hillslopes. Bell and Trangmar (1987) present an in-depth study of regolith materials and erosion processes for slopes on the western side of Banks Peninsula but no temporal constraint (i.e. absolute dating) is provided for deposition of colluvial sediments, emplacement of prehistoric rockfall, or removal of slope vegetation. The general effects of climate on slope process are considered but conditions of paleoenvironments (i.e. vegetation and climate) at the time of loess and loess-colluvium deposition is not discussed.

2.2 Paleoclimate and paleovegetation of Banks Peninsula

The understanding of past climate and vegetation in Banks Peninsula is increasing (e.g. Wilson, 1993; Shulmeister et al. 1999; Soons et al., 2002), but establishing temporal bounds for local and regional climate/vegetation flux remains a primary challenge. Shulmeister et al. (1999) employed a multi-technique approach (e.g. radiocarbon dating, thermoluminescence) supported by proxy data (diatoms, phytoliths, pollen) to show that pre-European flora of Banks Peninsula was dominated by mixed podocarp broadleaf

forests during interglacial periods and replaced by tall shrubland of mixed montane and coastal affinities during cooler glacial phases. Pollen diagrams from South Island consistently show a transition from grassland to shrubland (during Late Glacial) to forest (i.e. podocarp/hardwood) around the Holocene boundary (Almond et al., 2008). Native forest in Banks Peninsula was modified by two separate phases of human activity, beginning with the Polynesians (Maori) ca. 700-800 years BP and continuing with the Europeans, who settled the area approximately 150 years ago (McWethy, 2010; Harding, 2003; McGlone 1989). By 1900, Europeans had removed >98% of the indigenous forest (Wilson, 2008; Wilson, 2013; Harding, 2003), leaving slopes vulnerable to accelerated erosion and mass wasting (Glade, 2003). Borella et al. (in review) demonstrate that anthropogenic deforestation on Banks Peninsula has increased the rockfall hazard by allowing modern boulders to travel further downslope.

3. Rapaki Study Site

The Rapaki study site (Figs. 1a-d) occupies the northern half of the southeastern slope of Mount Rapaki (Te Poho o Tamatea), situated above Rapaki village on the western side of Banks Peninsula. The hillslope is slightly concave with a total area of approximately 0.21 km^2, and consists of steep to subvertical bedrock cliffs composed of distinct sub-horizontal packages of massive, vertically jointed basaltic lava separated by indurated volcanic breccias. The bedrock cliffs are ~60 meters tall and ~300 meters wide. A ~23° sloping grassy hillslope composed of windblown loess, loess and volcanic colluvium, and overlying prehistoric and modern rockfall boulders is situated below the bedrock cliffs. Rapaki village lies at the hillslope base, from approximately 70 meters (asl) to sea level. The removal of slope vegetation (i.e. native forest) has left the existing hillslope vulnerable to mass wasting and gulley formation (Fig. 1c).

Rockfall deposits sourced from the upslope bedrock cliffs are a dominant surface feature at Rapaki (Fig. 1c). More than 650 individual modern boulders ranging in diameter from <15 cm to >3m were dislodged from the bedrock source cliffs near the top of Mount Rapaki in the 22 February and 13 June 2011 Canterbury earthquakes (Massey et al.,

2014; Heron et al., 2014; Mackey and Quigley, 2014; Borella et al, in review). Twenty-six (26) of these boulders, ranging in volume from ~0.25 m^3 to ~28.0 m^3, impacted Rapaki village. Individual boulders (Fig. 1d) travelled up to 770±15 m downslope from the source cliff. Prehistoric rockfall deposits are found interspersed with modern rockfall and are more abundant at Rapaki, where we mapped and characterized 1543 rocks ranging in volume from 0.001 m^3 to >100 m^3 (Borella et al., in review). Prehistoric rockfall deposits (Figs. 2-7) are distinguishable from modern rockfall deposits because they are partially embedded in hillslope colluvium, are visible in pre-Canterbury Earthquake Sequence (CES) imagery, exhibit a high degree of surface roughness in volcanic breccia boulders due to differential weathering between basaltic clasts and finer-crystalline host matrix, and have surfaces with extensive lichen cover (Mackey and Quigley, 2014; Borella et al., in review). Mackey and Quigley (2014) used cosmogenic ^{3}He surface-exposure dating on 19 paleo-boulder surfaces to determine the emplacement time of prehistoric rockfall at Rapaki and constrain the temporal distribution and likely sources of past strong ground shaking analogous to that of the moment magnitude M_w 6.2 February 22 and M_w 6.0 July 13, 2011 Christchurch earthquakes. Prehistoric rockfall was attributed to a strong proximal earthquake at ca. 8-6 ka, with another potential prehistoric rockfall event occurring ca. 14-13 ka.

4. Methods

4.1 Stratigraphic analysis and sampling

Selection of prehistoric boulders and adjacent trench locations for stratigraphic analysis and sampling were chosen based upon the following criteria:

(1) The prehistoric boulder should be large enough (>5.0 m^3) to ensure sufficient subaerial exposure and sufficiently buried to ensure post-emplacement stability; (2) be located on an interfluve (relative topographic high) to help limit post-emplacement mobility and sediment depositional complexities; (3) have a well-developed and thick colluvial wedge at the boulder backside with no evidence of pervasive late-stage tunnel

gulley erosion or anthropogenic and livestock modification; and (4) have a Mackey and Quigley (2014) surface exposure age so that cross-validation between luminescence and CN surface exposure dating methods can be performed.

Prehistoric boulders with widely ranging (~8-27 ka) CN surface exposure ages were targeted to test the hypothesis that colluvial sediments and geomorphic processing in the study site is Holocene in age and any pre-Holocene rockfall boulders are likely buried beneath colluvium. Four prehistoric boulders (PB2-PB5) were chosen for detailed investigation at Rapaki (Fig. 1b,c). Two additional trenches were excavated adjacent to PB1 and PB6 (see Supp. Figs.1 and 2).

4.2 Dating Methods

4.2.1 Luminescence Dating

Thirteen samples were collected for luminescence dating in (i) loess and loess-colluvium deposits underlying the prehistoric boulders and (ii) loess-colluvium accumulated behind the boulders after emplacement on the hillside (Sohbati et al., in review). Sampling was conducted by pushing 5-cm-diameter stainless-steel tubes (with 15 cm length) into cleaned sections of the trench walls. To constrain emplacement timing for each of the prehistoric boulders, samples were collected within sediments lying directly below (maximum age) and above (minimum age) what was determined to be the existing ground surface at the time of boulder fall.

Luminescence samples were analyzed at The Nordic Centre for Luminescence Research in Roskilde, Denmark. Luminescence sample preparation and analytical details are provided in Sohbati et al. (in review). Optical ages are labeled on corresponding trench logs (Figs. 2c,3c,4c,6c,7b) and presented in Table 1.

4.2.2 Radiocarbon Dating

^{14}C dating of charcoal was performed on four samples to constrain the depositional age of the host colluvial sediments. We use the charcoal dates as a proxy for timing of sediment deposition, assuming that erosion, transport, and deposition of the charcoal-containing sediment occurred shortly after burning. Charcoal was retrieved near the base of the most recent colluvial sediments (LC-2_R) in PB3 and PB4. Charcoal samples ranging between 70 and 500 mg were submitted to the Rafter Radiocarbon Laboratory in Wellington, New Zealand, for accelerator mass spectrometry (AMS) radiocarbon analysis. Conventional ^{14}C age (years BP) is reported as defined by Stuiver and Polach (1977). Ages were calibrated using the Southern Hemisphere calibration curve (SHCal13; Hogg et al., 2013). We report both 2σ and 1σ calendar-calibrated ^{14}C age ranges in the text and Table 2 (see also Supp. Figs. 3-6). Conventional ^{14}C ages are also presented in Table 2. A more detailed description of the radiocarbon dating methodology is presented in the Supplementary Information section.

4.3 Phytoliths

Phytolith analysis was performed on PB2 loess and loess-colluvium. A single sample was collected from the in-situ loess, while top and bottom samples were collected within LC-1 and LC-2 units. Five sub-samples were collected from each field sample bag in the laboratory for phytolith analysis. Extraction of phytoliths followed the method of Carter (2000). Organic material was removed by heating each sample in 25% H_20_2 for ~72 hours. H_2O_2 was then washed off by the addition of 40 mL distilled water, and then centrifuged three times at 2500 rpm for 10 minutes. The residue was wet-sieved at 250 μm and the coarser material discarded. Samples were then heated in an oven at 40°C for 24 hours to reduce moisture content. Phytoliths were isolated by adding heavy liquid lithium heteropolytungstate (LST; specific gravity of 2.13 g/mL) to rinsed samples, mixed to suspend particles, and centrifuged for 10 minutes at 2000 rpm. Phytolith classification followed the method developed by Carter (2007), and Banks Peninsula flora was identified using Wilson (2012). Approximately 100-150 phytolith forms were counted per sample (total=592) and then converted to percentages. Phytolith results are presented in Fig. 8, Fig. 9, and Table 3.

5. Results

5.1 Trench stratigraphy

5.1.1 In-situ Loess

The in-situ loess is the oldest sediment observed within each of the exploratory trenches and predates emplacement of the studied boulders (Figs. 2-7). It consists of a light yellowish brown to light olive brown, massive, hard, and dry silt to sand loam and contains essentially no (≤0.2%) sediment derived from the proximal volcanic source rock (i.e. basalt) (Table 4a-d and Supp. Table 1). The loess exhibits characteristic gammate structure with grey fissures/veins and desiccation cracks with infilling translocated clay, as well as calcite-filled tubular root structures.

5.1.2 LC-1 (Phase 1 Colluviation)

LC-1 postdates in-situ loess deposition and pre-dates emplacement of the studied prehistoric boulders. It represents the oldest of the loess colluvial units and is comprised of a light olive brown to grayish brown to light yellowish brown, massive to very poorly layered, hard, dry to occasionally damp, silt loam with minor (≤1%) gravel, pebble, and cobble sized material derived from the proximal volcanic source rock (Table 4a-d and Supp. Table 1). The presence of volcanic derived coarse-grained material marks the primary difference between LC-1 and the underlying *in-situ* loess, and is reflective of a shift from wind to water dominated deposition.

A distinct paleosol exists within the upper section (i.e. PB2, PB3) or spans the entirety (i.e. PB4, PB5) of LC-1. Paleosol development is most advanced within PB2, PB4, and PB5 (maximum thickness ~44 cm) LC-1 sediments, and displays abundant mottling, clay coatings/worm casts, mm-scale voids (burrows, dissolved roots), calcite-filled desiccation cracks, and in some cases, increased clay content (see Table 4a-d and Supp. Table 1).

Paleosol thickness is generally observed to be consistent adjacent to and beneath the boulders, with the exception of PB2, where the paleosol thins to a minimum beneath the boulder.

An irregular unconformity is observed at the top of LC-1 within each of the exploratory trenches, marking an extended time period during which non-deposition and/or erosion occurred at the boulder locations (Figs. 2-7). This surface marks the boundary between sediments that pre-date boulder emplacement (LC-1) and those accumulating after deposition (LC-2) of the studied boulders. We interpret this surface as the paleo-ground surface at the time of boulder emplacement and its continuance can be observed directly beneath PB2-PB5. We used differences in texture, density, color, and moisture content between the older LC-1 sediments and younger LC-2 deposits to identify the unconformity.

5.1.3 LC-2 (Phase II Colluviation)

LC-2 accumulation post-dates prehistoric boulder emplacement and is observed behind each of the studied boulders as a well developed, ~50-130 cm thick, colluvial wedge. LC-2 matrix consists of a grayish brown to brown to dark grayish brown, massive to poorly layered, soft to firm, damp to semi-moist, silt loam (Table 4a-d). Gravel-sized ‘stones’ (3-6 mm diameter) are commonly encountered within the predominantly silty matrix. We observe a marked increase in volcanic-derived (basaltic) material within LC-2 (see Supp. Table 1), ranging in size from medium to coarse-grained sand and gravel to pebble and small boulder sized volcanic rocks. Maximum percent for volcanic derived earth material is ~17%. LC-2 sediments reflect deposition by increased overland flow process and mass wasting (e.g. debris and mud flows), implying a period of less stable slope conditions. LC-2 contains abundant small rootlets and pervasive yellowish brown to brownish yellow mottling. From the perspective of soil development, LC-2 gives the appearance of several stacked A-horizon soils that were unable to further develop due to relatively high sediment accumulation rates that exceeded soil formation rates behind each of the studied boulders.

5.1.4 LC-2_R (Phase III Colluviation)

LC-2_R represents the latest phase of LC-2 colluviation and is observable within the PB3 and possibly PB4 exploratory trenches (Figs. 3b,c; 4b,c). LC-2_R post-dates boulder emplacement and records anthropogenic forcing at Rapaki. In PB3, LC-2_R is comprised of a grayish brown to very dark gray, poorly to moderately layered, soft, dry to slightly damp, silt loam with minor gravel (Table 4b and 4c). Charcoal was observed within the lower 30 cm and within sediment wrapped and deposited around the sides of PB3 (at base). Radiocarbon dates for the charcoal fragments are presented in Table 2 and Supplementary Figs. 3-5. At approximately 52 cm downward from the ground surface, charcoal is mixed with small fragments of orange to reddish orange charred brick/pottery, indicating possible later European burning and suggesting that colluvium above this level occurred during European settlement. For PB4, we propose the upper ~35-50 cm of LC-2 may be roughly time equivalent to the LC-2_R sediments observed in PB3. A 1-2 mm fragment of charcoal has been logged at a depth of ~33 cm from the existing ground surface. Radiocarbon dating of the charcoal fragment has been performed (see Table 2 and Supp. Fig. 6).

5.1.5 Infill Events

Infill events post-date boulder emplacement and deposition of adjacent LC-2 sediments. Two separate infill events (IF-1 and IF-2) are observed at the boundary between PB2 and LC-2 colluvial wedge sediments (see Fig. 2c and Table 4a). We propose that space created at the back of PB-2 for infilling may have resulted from several processes including (1) minor shifting of the boulder during earthquake-induced strong ground shaking, (2) desiccation and subsequent contraction of sediment adjacent to PB2, and/or (3) erosion of pre-existing sediment at the boulder-sediment boundary. It is possible that I-1 and I-2 record two separate prehistoric shaking events and subsequent infill deposition. A single infill (IF-1) event is observed adjacent to PB4 (see Fig. 5) and consists of dark gray sandy silt (Table 4c). The sediment appears recent and has filled in

space created adjacent to the boulder backside. PB4 infill is similar in character (i.e. texture, composition) to IF-2 observed in PB2 trench sediments. PB4 records only a single infill event and may reflect a higher in-situ stability or younger emplacement age compared with PB2. No late infilling events are observed at the boundary between the LC-2 colluvial wedge sediments and upslope side of the PB3 and PB4.

5.2 OSL and Radiocarbon Chronology

5.2.1 PB2

The OSL age for ROSL-07 indicates latest *in-situ* loess was deposited 27.2±3.0 ka and agrees well with the quartz OSL age from ROSL-02 (quartz=29.3±2.5) (see Table 1 and Supp Fig. 1). Age agreement also exists between the ROSL-02 quartz OSL and K-feldspar (K-feldspar=28.5±1.6 ka) ages, suggesting the anomalously young K-feldspar age for ROSL-07 (21.8±1.4 ka) is unreliable. Optical ages within middle and upper sections of LC-1 indicate deposition between 12.0±1.4 and 12.5±1.1 ka (quartz ages) and 10.2±0.6 and 10.8±0.6 ka (K-feldspar ages) (Fig. 2c). We attribute the similarity and overlap (apparent inversion) in ages between the upper (ROSL-05) and lower (ROSL-06) samples to reflect rapid sediment deposition during this time period. The presence of a well-developed paleosol within the upper ~13-34 cm of LC-1 (Fig. 2b,c) indicates a period of relative stability and minimal sediment input subsequent to LC-1 deposition. The significant time interval (~4.8 ka - quartz OSL ages; ~3.9 ka - K-feldspar OSL ages) separating latest LC-1 and earliest LC-2 deposition (Figs. 2c and 10) suggests the LC-1/LC-2 boundary represent an unconformity. Quartz and K-feldspar OSL ages (ROSL-04) indicate earliest deposition of LC-2 occurred 7.7±0.8 and 6.9±0.4 ka, respectively (Fig. 2c).

5.2.2 PB3

Optical ages for ROSL-09 indicate latest preserved deposition of LC-1 occurred ca. 5.8±0.5 ka (quartz) or 6.5±0.4 ka (K-feldspar) (Fig. 3c). This age range represents the

youngest for deposition of LC-1 among the four studied prehistoric boulders. We note that soil development in PB3 LC-1 sediments is not as advanced as that observed in LC-1 sediments beneath PB2, PB4, and PB5. However, this is consistent with its younger depositional age and corresponding shorter time window (~2.9-3.9 ka) for soil development. Optical ages for ROSL-08 suggest deposition of LC2 occurred at approximately 2.9±0.3 ka (quartz) or 2.6±0.2 ka (K-feldspar) (Fig. 3c).

Radiocarbon dates are generated from three charcoal samples retrieved within the lowest horizon of LC-2_R (Fig. 3c, Table 2 and Supp. Figs. 3-5). The 2-sigma calibrated ages (calendar yr A.D.) range from AD 1664 to AD 1950, with the highest sub-interval probability from AD 1724 to AD 1809 for Rap-CH01 (70.4% of area), AD 1722 to AD 1810 for Rap-CH03 (63.8%), and AD 1732 to AD 1802 for Rap-CH05 (79%). A fire event (or sequence of events) occurring sometime between ~1722 AD and 1810 AD predates European settlement and is consistent with the localized burning during the late Maori Period (~AD 1600–1840) as proposed by McWethy et al. (2010). Assuming sediment deposition occurred shortly after burning of slope vegetation, earliest LC-2_R sedimentation occurred between ~200 and 300 years ago. Charcoal observed stratigraphically higher than the sampled locations exhibit fragments of brick/pottery mixed with charcoal and probably represents a later phase of European burning (Fig. 3c).

5.2.3 PB4

The optical ages at the top and bottom of LC-1 indicate deposition between 13.4±1.2 and 10.3±1.1 ka for quartz, and 12.7±0.7 and 10.4±0.7 ka for K-feldspar (Fig. 4c). Luminescence ages obtained above and below the LC-1/LC-2 boundary suggest a depositional hiatus of ~6.1 (quartz) or ~6.6 (K-feldspar) ka. Luminescence dating indicates earliest LC-2 accumulation occurred 4.2±0.4 ka (quartz) or 3.8±0.2 ka (K-feldspar) (Fig. 4c).

The radiocarbon age from charcoal sample Rap-CH06 suggests latest LC-2 sedimentation occurred sometime between AD 1677 and AD 1950. An analysis of 2σ and 1σ

confidence intervals (Supp. Fig. 6) further indicates that late LC-2 (possibly LC-2_R) deposition most likely occurred between AD 1836 and AD 1884, coincident with European arrival in the area and a shift into anthropogenically-influenced sediment accumulation at Rapaki.

5.2.4 PB5

Luminescence ages at the top of LC-1 indicate latest deposition of pre-boulder emplacement loess-colluvium occurred 10.2±0.8 ka (quartz) or 12.6±0.8 ka (K-feldspar) (Fig. 6c,7b). The initiation of LC-2 deposition began at 1.7±0.2 ka (quartz) and 1.9±0.1 ka (K-feldspar). Ages from above and below the LC-1/LC-2 contact suggest a depositional hiatus of ~8.5 ka (quartz OSL) or ~10.7 ka (K-feldspar OSL) at the PB5 location, the longest of the studied boulders (Fig. 10).

5.3 Sedimentation rates

Table 5 presents results for linear accumulation rates for colluvium deposited behind and below (where applicable) PB2-PB5. Optical and radiocarbon samples names and ages are shown, as well as the measured stratigraphic thickness between the bracketing ages. Temporal distributions may reflect differences in rates and processes of deposition between near-instantaneous debris and mud flow deposits and more gradual overland flow erosion and deposition. In consideration of this, the deposition rates represent only a first-order approximation, but serve to highlight changes in sediment accumulation through time. Our results suggest an overall increase in sediment accumulation rates moving stratigraphically upward, with a dramatic increase in depositional rate during Phase III colluviation.

5.4 OSL constraints on timing of boulder emplacement

Quartz OSL ages suggest PB2 was emplaced after 12.5±1.1 ka and before 7.7±0.8 ka (Fig. 10). K-feldspar ages constrain timing of PB2 emplacement to between 10.8±0.6 and

6.9±0.4 ka (Fig. 10). The top surface of PB2 yields a Mackey and Quigley (2014) CN surface exposure age of 13.0±2.3 ka (Fig. 2c and Fig. 10). Assuming the calculated experimental error for both methods, the CN age and optical ages show statistical overlap and can be used to further constrain the emplacement timing of PB2. Combining CN and quartz OSL ages suggests emplacement of PB2 after ~13.6 ka and before ~10.7 ka (Fig. 10). Comparison of CN and K-feldspar ages indicates PB2 emplacement after ~11.4 ka and before ~10.7 ka (Fig. 10). Given that the median CN surface exposure age is higher than the OSL maximum ages for the underlying sediment, it is possible that the surface exposure age is slightly overestimated. The consistency of the quartz and K-feldspar luminescence ages indicates the reliability of the two methods and adds further credibility to the luminescence ages.

Quartz OSL ages constrain timing of PB3 to after 5.8±0.5 and before 2.9±0.3 ka (Fig. 10). K-Feldspar IRSL ages constrain timing of PB3 emplacement to between 6.5±0.4 and 2.6±0.2 ka (Fig. 10). The top surface of PB3 has a CN surface exposure age of 8.1±2.1 ka (Mackey and Quigley, 2014) (Fig. 3c and Fig. 10). The CN age and luminescence ages do show agreement (i.e. statistical overlap). Combining CN and quartz OSL ages suggests emplacement of PB3 after ~6.3 ka and before ~6.0 ka (Fig. 10). Combining CN and K-feldspar OSL ages indicates PB3 emplacement after ~6.9 ka and before ~6.0 ka (Fig. 10). We note again that the median CN age for PB3 plots well above the maximum OSL age (including error margin), indicating that surface exposure age may overestimate the boulder emplacement age.

Quartz OSL ages suggest PB4 was emplaced after 10.3±1.1 and before 4.2±0.4 ka (Fig. 10). K-Feldspar IRSL ages constrain timing of PB4 to after 10.4±0.7 and before 3.8±0.2 ka (Fig. 10). The top surface of PB4 has a CN surface exposure age of 26.9±2.9 ka (Mackey and Quigley, 2014) (Fig. 4c and Fig. 10). The OSL ages are not consistent with the surface exposure age and strongly suggest that PB4 CN surface exposure age reflects pre-detachment inheritance (Fig. 10). In middle and footslope positions it is likely that any boulder emplaced 26.9 ka would be buried beneath *in-situ* loess and loess-colluvium deposits.

Quartz OSL ages constrain timing of PB5 to after 10.2±0.8 and before 1.7±0.2 ka (Fig. 10). K-feldspar ages constrain timing of PB5 to after 12.6±0.8 and before 1.9±0.1 ka (Fig. 10). The top surface of PB5 has a CN surface exposure age of 15.7±2.3 ka (Fig. 5c and Fig. 10). The optical ages are not consistent with the surface exposure age and strongly suggest that PB5 CN surface exposure age reflects pre-detachment inheritance (Fig. 10).

Treated independently, the maximum and minimum luminescence ages suggest it is possible PB2-PB5 were emplaced during a single rockfall event occurring ca. 8-6 ka (Mackey and Quigley, 2014). However, it is equally plausible the boulders were emplaced during two or more prehistoric rockfall events. The combination of optical and CN ages suggests at least two separate prehistoric rockfall events at ~8-6 ka and ~14-12 ka, as proposed by Mackey and Quigley (2014) (Fig. 10).

5.5 Phytolith Sequence

Phytolith analysis was performed on PB2 *in-situ* loess and loess-colluvium to provide information on vegetation changes at the Rapaki study site in response to climate for the last ~27 ka. The assumption is made that the extracted phytoliths represent the vegetation growing during the time (see Figure 2c) of loess and loess-colluvium deposition. The phytolith results are shown in Figs. 8 and Table 3. Major phytolith morphological forms are shown in Fig. 9.

5.5.1 PS1 (*in-situ* loess)

PS1 (*in-situ* loess) (luminescence depositional age ~27 ka) is dominated by globular granular (35%), globular echinate (28%), and variety of graminoid phytoliths including elongate long cell (13%) and cuniform bulliform cell (9%) types (Fig. 8 and Table 3). Globular granular phytoliths indicate a tree/shrub origin, globular echinate phytoliths reflect a palm origin, and graminoid phytoliths suggest a grass origin (Carter, 2007; Carter, 2000). Based upon the high abundance of tree/shrub (~40%) and grass (~32%)

phytoliths (Table 3), a cool temperate environment is interpreted, although the presence of globular echinate (~28%) phytoliths implies temperatures 'warm' enough for palm growth.

5.5.2 PS2 (lower LC-1)

In PS2 (~13-11 ka), graminoid phytoliths, including trapeziform polylobate (20%) and elongate long cell (18%) are found in highest percentage (43%), followed by globular echinate (33%) and globular granular (16%) phytolith varieties (Fig. 8, Table 3). Relative to PS1 phytolith assemblages, we observe increases in the growth of grass (+11%) and palm phytoliths (+5%), and a notable decline (-16%) in tree/shrub forms. The decrease in tree/shrub species and increase in grass phytolith types could reflect a shift into a 'cooler' climate condition. However, the continued presence and increase of palm phytoliths suggests warm temperate elements (i.e. warm microclimates near the sea) existed. We propose a similar cool to maritime environment with warm temperate elements.

5.5.3 PS3 (upper LC-1)

Globular echinate phytoliths (41%) are found in highest percentage within PS3 sediments (~13-11 ka). Graminoid phytoliths are also abundant (37%) but show a corresponding decrease (-6%) relative to PS2 (Fig. 8, Table 3). Phytoliths of tree/shrub origin show a similar percentage (22%) to PS2 (Table 3). The progressive increase of globular echinate phytoliths (palm origin) suggests a shift into a warmer, wet and humid climate, consistent with the observed well-developed paleosol in the top of PB2 LC-1 sediments (Fig. 2c).

5.5.4 PS4 (lower LC-2)

PS4 sediments (~8-7 ka) contain high percentages of globular granular (31%), globular echinate (27%), and elongate long cell (22%) phytolith assemblages (Fig. 8 and Table 3). We observe a marked increase in tree/shrub phytoliths (+18%), and a decline in palm (-14%) and grass species (-4%). We interpret the increase in globular granular phytoliths

(trees/shrubs) and decrease in palm trees to indicate a shift back into a maritime cool temperature climate. The most abundant tree species were probably thinbarked totara (P. hallii) with broadleaf (Griselinia littoralis) and cedar (Libocedrus bidwillii).

5.5.5 PS5 (upper LC-2)

PS5 (~3-2 ka) is dominated by globular echinate phytoliths (68%) (Fig. 8, Table 3), indicating abundant palm growth and a probable shift into a wet, humid, and warm environment. The most abundant species were probably nikau palm (*Rhopalostylis sapida*) and akeaka (*Dodonaea viscosa*). Transition into a wet and warm climate is consistent with an increasing sediment accumulation rate during the late-Holocene. The dramatic increase in palm phytoliths (+41%) is accompanied by a marked reduction in tree/shrub phytolith assemblages (-30%) relative to sample PS4. Graminoid phytoliths are also reduced (-11%) during this time.

The phytolith results are used to infer vegetation changes spanning ~27 ka to present and suggest that paleo-vegetation at Rapaki fluctuated within an overall cool to maritime cool temperate zone with warm-temperate elements. The data suggests that the Rapaki hillslope remained vegetated through the late Pleistocence and Holocene epochs, prior to the occurrence of Maori and European deforestation in Banks Peninsula. Grasses and tree/shrub species dominated during colder periods, while nikau palm was most abundant during warmer climate phases (i.e. ~12-11 ka and ~3-2 ka). Grasses remained relatively stable throughout climate fluctuations.

6. Discussion

6.1 Rapaki landscape evolution, paleo-vegetation, and paleo-climate

Stratigraphy and OSL and radiocarbon chronologies reveal shifts in landscape evolution spanning the LGCP (~28-18 ka), LGIT (~18-11.6 ka), and Holocene interglacial period (~11.6 ka to present) (cf. Alloway et al., 2007).

Quartz OSL ages indicate *in-situ* loess was accumulating at Rapaki around ~29-27 ka (Table 1). Our phytolith analysis suggests this period was dominated by tree/shrub and grass phytolith forms, implying cool temperature conditions. However, the presence of palm phytoliths at this time is surprising, and perhaps suggests 'warmer' climate conditions than previously thought (e.g. Shulmeister, 1999; Soons et al., 2002) during the beginning of the last glacial coldest period. Alloway et al. (2007) describe a warmer and more variable climate phase between ca. 27 and 21 cal. yr BP in New Zealand. Hughes (2008, 2010) also provides evidence from diatoms (from Charwell basin, Canterbury) suggesting the LGM and LGIT were relatively wet periods, at least locally, thus highlighting the potential for warmer microclimates in the eastern South Island.

Phase 1 colluviation reflects a period of relative slope stability, where deposition by overland flow processes predominated. Based upon the small amount of coarse-grained volcanic derived sediment and the absence of large rockfall boulders, mass wasting was apparently a limited mechanism for landscape evolution during this time, at least in the studied boulder locations. The small increase in volcanic sediment (~1-3%) (relative to *in-situ loess)* could reflect a slight warming of climate and corresponding increase in precipitation and weathering of volcanic bedrock with transition into the Holocene. Phytoliths within upper LC-1 sediments suggest a high abundance of palm trees and a shift into a warmer, wet, and humid climate ca. 12 ka (late Pleistocene-Holocene boundary) – consistent with the transition into a more stable depositional period during which the observed paleosol developed. Surprisingly, tree/shrub phytoliths remain in relatively low abundance (22%) even as palm growth increases. It is possible that the relative percentage of tree/shrub phytoliths is underestimated, due to poor phytolith preservation, and was more prevalent during this time. Carter (2007) notes that tree/shrub phytoliths are notorious for their poor preservation, especially for polyhedral phytolith morphologies.

Luminescence ages suggest a period of non-deposition (and possibly erosion) ranging from ~3 to ~9 ka occurred at Rapaki after deposition of LC-1 sediments. Maximum and

minimum luminescence emplacement ages indicate the PB2, PB3, PB4, and PB5 unconformities have different temporal ranges (Fig. 10). It is possible that the PB2, PB4, and PB5 unconformities were initiated around the same time, with the break in sedimentation occurring ~10-11 ka. Alternatively, the depositional hiatus in the area of PB2 may have been initiated earlier, approximately ~12.5 ka. The break in colluvial deposition at the PB3 location occurred later around ~6 ka. We propose the unconformities have resulted primarily from local variable hillslope conditions rather than a larger-scale regional factor (e.g. climate cooling), although higher frequency climate conditions (i.e. storms) certainly influence hillslope deposition.

Paleosol development is most advanced within PB2, PB4, and PB5 trenches, perhaps reflecting their relatively long exposure periods (~5-8.5 ka) compared with PB3 (~3 ka). The abundance of worm casts (i.e. clay coatings) and old roots and root traces (found primarily within the thin upper section) are consistent with an ancient A horizon soil, although Rapaki paleosols also exhibit characteristics indicative of B soil horizon development, including intense mottling (i.e. iron and aluminum) and a distinct structure highlighted by numerous vertical desiccation cracks. Field observations suggest an increase in clay content, although this is not supported by the grain size analyses. We propose that PB3, PB4, and PB5 were deposited after soil development, because the paleosol can be observed directly beneath each of the boulders and has a similar thickness to adjacent sections of the ancient soil not covered by the prehistoric boulders. The exception is PB2, where the paleosol thins beneath the boulder, suggesting its deposition closer to the maximum luminescence emplacement age.

Phase II colluviation (LC-2) reflects a period of relative slope instability. LC-2 deposits reflect a combination of mass wasting (e.g. rockfall, debris flow, mud flow) and overland flow processes. The increase in volcanic derived earth material (i.e. coarse-grained sand to large boulder fragments) may result from increased precipitation (i.e. causing erosion of volcanic source rock), but also rockfall likely generated during episodes of strong prehistoric seismic shaking (i.e. Mackey and Quigley, 2014; Borella et al., in review). As evidenced by the 2010-2011 CES, large quantities of volcanic rock are introduced into

the hillslope depositional system during strong proximal seismic shaking. Earliest deposition of LC-2 sediments occurred during the early to mid-Holocene and is recorded behind PB2, while deposition behind PB3, PB4, and PB5 occurred later around ~4-2 ka. LC-2 sediments are thinnest and accumulation occurs latest behind PB5, indicative of its position on an interfluve, where deposition of sediment was limited. Early to mid-Holocene LC-2 sediments accumulated at a rate of 0.07-0.08 mm/a, while late-Holocene sediment accumulated at a higher rate of 0.16-0.27 mm/a. This indicates a progressive increase in accumulation rate consistent with Holocene warming and increased erosion and sediment accumulation at least partially attributed to high sedimentation rates following deforestation of the Rapaki hillslope sometime after ~1661 AD. Phytolith assemblages within Holocene sediments indicate a probable cool temperate environment in the early to mid-Holocene with warming and corresponding maximum palm production (~68%) in the late Holocene period. The transition into a wetter and warmer climate is consistent with increasing accumulation rates in late-Holocene hillslope sediments. Grass and tree/shrub phytolith forms are in apparent decline during this time (~3 ka), although percentages could be underestimated due to poor preservation.

Phase III colluviation ($LC\text{-}2_R$) is recorded in the youngest colluvial wedge sediments accumulated at the backside of PB3 and possibly PB4, and marks the first evidence for anthropogenic influence on the Rapaki landscape. Burning of the hillslope vegetation would have (i) reduced surficial slope stability and increased erosion by removing stabilizing root systems and (ii) generated abundant organic debris for transport. The dramatic increase in sediment accumulation rate during Phase III colluviation is consistent with rapid erosion and downslope colluvial deposition following anthropogenic burning of Rapaki hillslope vegetation.

6.2 Efficacy of OSL method for dating prehistoric rockfall and future implications

We demonstrate that optical dating of loessic hillslope sediments can successfully constrain timing of prehistoric boulder emplacement (Sohbati et al., in review), which, under certain circumstances, may be used as a proxy for the temporal occurrence of

prehistoric earthquakes (Mackey and Quigley, 2014). However, the temporal resolution is limited by the episodic and spatially irregular nature of hillslope sedimentation, highlighting a challenge when using hillslope sediments to constrain timing of prehistoric rockfall and establish paleo-shaking chronologies. A comparison of the luminescence ages shows quartz OSL ages provide a time window (i.e. difference between maximum and minimum ages) for boulder emplacement ranging from 2.9 to 8.5 ka (range=5.6 ka), while K-feldspar OSL ages offer a resolution between 3.8 and 10.7 ka (range=6.8) (Figure 10). Based upon these results, optical dating of hillslope sediments in the Port Hills has the potential to reveal prehistoric rockfall events with recurrence intervals ranging from ~3 to ~9 ka. Resolution of higher frequency rockfall events (< 3 ka) will require a more favorable depositional system (e.g. more constant hillslope sedimentation) and/or improvements in selecting boulder locations and luminescence sampling for maximum and minimum emplacement ages.

Temporal constraints for boulder fall timing could possibly be improved by sampling sediment closer to the LC-1/LC-2 contact (i.e. unconformity, boulder emplacement surface). We generally sampled ~10-15 cm below and above the LC-1/LC-2 surface because its exact position was often difficult to determine. In addition, sediment directly beneath (and adjacent to) the boulder (<10 cm) was found to be highly weathered, and as a result, we avoided sampling it because we were concerned the samples would yield unreliable ages. However, luminescence ages from within the LC-1 paleosol horizon (i.e. ROSL-05,-09,-11,-12,-14) are in stratigraphic order and make geologic sense (Sohbati et al., in review), suggesting that sampling closer to the unconformity could yield accurate luminescence ages and provide a tighter temporal constraint for boulder emplacement timing.

Our results indicate areas that are topographically high (relative to nearby areas) and receive low sediment input, are less desirable (e.g. PB5 location) for using luminescence dating to constrain timing of boulder emplacement. Similarly, but for different reasons, boulders located in drainage valleys/gullies should be avoided due to potential boulder mobility issues and depositional complexities (i.e. frequent deposition and removal of

sediment behind boulders). The former eliminates the boulder as a viable candidate for optical dating, while the latter reduces the minimum age constraint for boulder emplacement.

Importantly, our ability to date prehistoric rockfall events older than ~13 ka is limited by sediment deposition on the Rapaki hillslope. We obtained no luminescence ages greater than 12.5±1.1 ka within the youngest LC-1 loess colluvium (maximum age constraint), suggesting that boulders emplaced before this time would likely be buried beneath loess-colluvial sediments at Rapaki (at least in midslope to footslope positions). This supports the conclusion by Mackey and Quigley (2014) that any boulders deposited before 17-13 ka are likely to be buried beneath the Rapaki hillslope sediments. Although some depositional variability is likely, we expect this will be the case throughout most of Banks Peninsula. Extensive trenching could be performed to expose buried rockfall boulders, but would require exploratory trenches of great depth and width (to ensure trench safety). It is probable that older rockfall boulders (i.e. deposited before ~13 ka) will be observable closer to the source rock, where erosion dominates and older boulders may remain exposed. However, erosion of sediment beneath and behind the boulders will make constraining boulder fall timing using optical dating of hillslope sediments difficult.

Our luminescence ages provide an independent method for cross-validating the ^{3}He cosmogenic surface exposure ages generated at Rapaki by Mackey and Quigley (2014) and effectively identify surface exposure ages that reflect pre-detachment inheritance (i.e. boulder surfaces not created during a prehistoric rockfall event). Combining CN surface exposure ages with luminescence ages has the potential to further constrain timing of boulder fall, as evidenced by PB2 and PB3. A comparison of OSL and CN ages, suggests it is a possibility that PB3 was deposited during the Mackey and Quigley (2014) proposed ~7±1 ka rockfall event, but PB2 was possibly not and may have occurred during an earlier rockfall event.

6.3 De-coupling of boulder emplacement and loessic colluvium deposition

Field observations combined with an examination of our luminescence and radiocarbon ages suggest that boulder emplacement and deposition of loessic colluvium at Rapaki are de-coupled and caused by different mechanisms. We propose rockfall is generated primarily by earthquake-induced strong proximal ground shaking (Mackey and Quigley, 2014), while erosion, transport, and deposition of loess colluvium is controlled mainly by climate flux (i.e. rainfall, storms). The build-up of sediment (i.e. colluvial wedge) behind the studied boulders and the lack of equivalent sediments at the boulder front suggests the boulders were in place prior to deposition of the loess colluvium and that emplacement of the rockfall boulders and deposition of loess colluvium were probably not synchronous. This is further supported by the large breaks in sedimentation reflected by the maximum and minimum luminescence boulder emplacement ages. Furthermore, CN surface exposure and minimum emplacement optical ages for prehistoric boulders at Rapaki indicate the absence of prehistoric boulders deposited after ~3 ka and prior to the 2010-2011 CES, suggesting that higher frequency climatic episodes (i.e. 100-, 500-, 1000-year storms/floods) are probably not generating the observed large (~5-30 m^3) rockfall at Rapaki.

This disconnect implies that seismologic and climatic/meteorological phenomena play different roles in shaping the modern Rapaki landscape. A correlation between earthquake triggered rockfalls and longer-term hillslope response may exist, but it is difficult to evaluate. Prehistoric earthquakes could cause destabilization of the hillslope (e.g. debris and mud flows), making colluvial sediments more vulnerable to erosion and downslope transport. However, this was not the case during the 2010-2011 CES, where we observed no evidence of earthquake-induced landsliding (excluding rockfall) at the Rapaki study site. Small (~10 meter wide, ~20 meter long, 1-2 meter depth) debris and mud flows were observed during fieldwork, but coincided with a 100-year storm/flood event during April of 2014. As demonstrated during the 2011 Christchurch earthquakes, strong proximal shaking episodes introduce a significant volume of small and large rockfall into the hillslope depositional system. However, its relative influence on hillslope response (including impact on colluvium deposition and erosion) requires further investigation.

7. Conclusions

Optical and radiocarbon dating of slope sediments successfully constrains the timing of prehistoric rockfall and reveals three distinct phases of hillslope colluviation at Rapaki, New Zealand. Under certain circumstances, our approach may be used as a proxy for determining the timing of earthquake-triggered rockfalls and hillslope responses to anthropogenic influence elsewhere in New Zealand and globally. Field observations and luminescence ages suggest boulder emplacement and deposition of underlying and draping loessic colluvium did not occur concurrently and probably result from different causal mechanisms, implying that seismologic and climatic phenomena play different roles in shaping the modern landscape. Our preliminary phytolith analysis suggests paleo-vegetation at the study site fluctuated within a predominantly cool temperate to maritime cool environment with warm-temperate elements. Periods of maximum warming are inferred at the late Pleistocene/early Holocene boundary (~12-11 ka) and within the late (~3-2 ka) Holocene, based upon the high relative abundance of palm phytoliths. Our study provides insights into the spatial and temporal patterns of hillslope evolution, highlighting the importance of a multi-technique approach in understanding the roles of climate and vegetation change, earthquakes, and humans on surface processes.

8. References

Alloway B.V, Lowe D.J., Barrell D.J.A., Newnham R.M., Almond P.C., Augustinus P.C., Bertler N.A.N., Carter L., Litchfield N.J., McGlone M.S., Shulmeister J., Vandergoes M., Williams P., NZ-INTIMATE Members. (2007). Towards a climate event stratigraphy for New Zealand over the past 30 000 years (NZ-INTIMATE project). *Journal of Quaternary Science* **30**: 9-35.

Almond, P. C., Shanhun, F. L., Rieser, U., & Shulmeister, J. (2007). An OSL, radiocarbon and tephra isochron-based chronology for Birdlings Flat loess at Ahuriri Quarry, Banks Peninsula, Canterbury, New Zealand. *Quaternary Geochronology* ***2***(1-4): 4–8. doi:10.1016/j.quageo.2006.06.002

Almond, P.C., Roering, J.J., Hughes, M.W., Lutter, F.S., Lebouteiller, C. (2008). Climatic and anthropogenic effects on soil transport rates and hillslope evolution. *IAHS Publication* **325**: 417-424.

André, M. (1997). Holocene Rockwall Retreat in Svalbard: A Triple-Rate Evolution. *Earth Surface Processes and Landforms* **22**(5): 423–440. doi:10.1002/(SICI)1096-9837(199705)22:5<423::AID-ESP706>3.3.CO;2-Y

Balescu, S., Ritz, J. F., Lamothe, M., Auclair, M., & Todbileg, M. (2007). Luminescence dating of a gigantic palaeolandslide in the Gobi-Altay mountains, Mongolia. *Quaternary Geochronology* **2**(1-4): 290–295. doi:10.1016/j.quageo.2006.05.02

Bell, D.H., & Trangmar, B.B. (1987). Regolith materials and erosion processes on the Port Hills, Christchurch, New Zealand: Fifth International Symposium on Landslides. *Lausanne, A.A. Balkema* **1**: 93-105.

Bertolini, G. (2007). Radiocarbon dating on landslides in the Northern Apennines (Italy): Landslides and Climate Changes. *ISBN 978-0-415-44318-0* pp. 73-80.

Borella, J. Quigley, M., Vick, L. (in review). Anthropocene rockfalls exceed limits of prehistoric predecessors. *Nature Geoscience*.

Bull, W. B., King, J., Kong, F., Moutoux, T., Phillips, W. M. (1994). Lichen dating of coseismic landslide hazards in alpine mountains. *Geomorphology* **10**(1-4): 253–264. doi:10.1016/0169-555X(94)90020-5

Carter, J. A. (2000). Phytoliths from loess in Southland, New Zealand. *New Zealand Journal of Botany* **38**(2): 325–332.

Carter, J. A. (2007). Phytoliths. *Encyclopedia of Quaternary Science*: 2257–2265. doi:10.1016/B0-44-452747-8/00212-X

Chapot, M. S., Sohbati, R., Murray, A. S., Pederson, J. L., & Rittenour, T. M. (2012). Constraining the age of rock art by dating a rockfall event using sediment and rock-surface luminescence dating techniques. *Quaternary Geochronology* **13**: 18–25. doi:10.1016/j.quageo.2012.08.005

Cordes, S. E., Stock, G. M., Schwab, B. E., Glazner, A. F. (2013). Supporting Evidence for a 9.6 ± 1 ka Rock Fall Originating from Glacier Point in Yosemite Valley, California. *Environmental & Engineering Geoscience* **19**(4): 345–361. doi:10.2113/gseegeosci.19.4.345

Fattahi, M.,Walker, R., Hollingsworth, J., Bahroudi, A., Nazari, H., Talebian, M., Armitage, S., Stokes, S. (2006). Holocene slip-rate on the Sabzevar thrust fault, NE Iran, determined using optically stimulated luminescence (OSL). *Earth and Planetary Science Letters* **245**: 673–684.

Forsyth P.J., Barrell D.J.A., Jongens, R. (2008). Geology of the Christchurch Area. 1:250 000 geological map 16. Lower Hutt, Institute of Geological & Nuclear Sciences.

Fuchs, M., & Lang, A. (2009). Luminescence dating of hillslope deposits—A review. *Geomorphology* **109**(1-2): 17–26. doi:10.1016/j.geomorph.2008.08.025

Fuchs, M., Fischer, M., & Reverman, R. (2010). Colluvial and alluvial sediment archives temporally resolved by OSL dating: Implications for reconstructing soil erosion. *Quaternary Geochronology* **5**(2-3): 269–273. doi:10.1016/j.quageo.2009.01.006

Fuchs, M., Lang, A., Wagner, G.A. (2004). The history of Holocene soil erosion in the Phlious Basin, NE-Peloponnese, Greece, provided by optical dating. *The Holocene* **14**: 334–345.

Fuller, I.C., Macklin, M.G., Richardson, J.M. (2015). The Geography of the Anthropocene in New Zealand: Differential River Catchment Response to Human Impact. *Geographical Research* **53**(3): 255-269. Doi10.1111/1745-5871.12121

Glade, T. (2003). Landslide occurrence as a response to land use change: a review of evidence from New Zealand. *Catena* **51**: 297-314.

Griffiths, E. (1973). Loess of Banks Peninsula. *New Zealand Journal of Geology and Geophysics* **16**: 657–675.

Harding, J.S. (2003). Historic deforestation and the fate of endemic invertebrate species in streams. *New Zealand Journal of Marine and Freshwater Research* **37**: 333-345.

Hampton, S.J., Cole, J.W. (2009). Lyttelton Volcano, Banks Peninsula, New Zealand: Primary volcanic landforms and eruptive centre identification. *Geomorphology* **104**: 284-298.

Hanson, P.R., Mason, J.A., Goble, R.J. (2004). Episodic Late Quaternary slopewash deposition as recorded in colluvial aprons, Southeastern Wyoming. *Quaternary Science Reviews* **23**: 1835–1846.

Heron, D., Lukovic, B., Massey, C., Ries, W., & McSaveney, M. (2014). GIS modelling in support of earthquake-induced rockfall and cliff collapse risk assessment in the Port Hills, Christchurch. *Journal of Spatial Science* **59**(2): 313-332.

Hogg et al. (2013). $SHCAL_{13}$ Southern Hemisphere Calibration, 0-50,000 years CAL BP. *Radiocarbon* **55**: 1889-1903.

Hughes, M. W., Almond, P. C., Roering, J. J., & Tonkin, P. J. (2010). Late Quaternary loess landscape evolution on an active tectonic margin, Charwell Basin, South Island, New Zealand. *Geomorphology* **122**(3-4): 294–308. doi:10.1016/j.geomorph.2009.09.034

Hughes, M. W. (2008). Late Quaternary landscape evolution and environmental change in Charwell basin, South Island, New Zealand. PhD Thesis, Lincoln University, New

Zealand.

Ives, D. (1973). Nature and distribution of loess in Canterbury, New Zealand. *New Zealand journal of geology and geophysics* **16**(3): 587-610.

Lang, A., Moya, J., Corominas, J., Schrott, L., & Dikau, R. (1999). Classic and new dating methods for assessing the temporal occurrence of mass movements. *Geomorphology* **30**(1-2): 33–52. doi:10.1016/S0169-555X(99)00043-4

Lang, A., Wagner, G.A. (1996). Infrared stimulated luminescence dating of archaeosediments. *Archaeometry* **38**: 129–141.

Lang, A.,Wagner, G.A. (1997). Infrared stimulated luminescence dating of Holocene colluvial sediments using the 410 nm emission. *Quaternary Science Reviews* **16**: 393–396.

Luckman, B.H., Fiske, C.J. (1995). Estimating long-term rockfall accretion rates by lichenometry. *Geomorphology* pp. 233– 255.

Mackey, B. H., Quigley, M. C. (2014). Strong proximal earthquakes revealed by cosmogenic ^{3}He dating of prehistoric rockfalls, Christchurch, New Zealand. *Geology* **42**(11): 975–978. doi:10.1130/G36149.1

Massey, C.I., McSaveney, M.J., Taig, T., Richards, L., Litchfield, N.J., Rhoades, D.A., McVerry, G.H., et al. Determining rockfall risk in Christchurch using rockfalls triggered by the 2010-2011 Canterbury earthquake sequence. *Earthquake Spectra* **30**(1) 155-181.

Matmon, A, Shaked, Y., Porat, N., Enzel, Y., Finkel, R., Lifton, N., Agnon, A. (2005). Landscape development in an hyperarid sandstone environment along the margins of the Dead Sea fault: Implications from dated rock falls. *Earth and Planetary Science Letters* **240**(3-4): 803–817. doi:10.1016/j.epsl.2005.06.059

McCarroll, D., Shakesby, R. A., Matthews, J. A. (2001). Enhanced rockfall activity during the litte ice age: Further lichenometric evidence from a Norwegian Talus. *Permafrost and Periglacial Processes* **12**(2): 157–164. doi:10.1002/ppp.359

McGlone, M.S. (1983). Polynesian deforestation of New Zealand: A Preliminary Synthesis. *Archaeology in Oceania* **18**: 11-25.

McGlone, M.S. (1989). The Polynesian settlement of New Zealand in relation to environmental and biotic changes. *New Zealand Journal of Ecology* **12**: 115–129.

McWethy, D.B., Whitlock, C., Wilmshurst, J.M., McGlone, M.S., Fromont, M., Li, X., Dieffenbacher-Krall, A., Hobbs, W.O., Fritz, S.C., Cook, E.R. (2010). Rapid landscape transformation in South Island, New Zealand, following initial Polynesian

settlement. *PNAS* **107**: 21343-21348.

Rinat, Y., Matmon, A., Arnold, M., Aumaître, G., Bourlès, D., Keddadouche, K., Finkel, R.C. (2014). Holocene rockfalls in the southern Negev Desert, Israel and their relation to Dead Sea fault earthquakes. *Quaternary Research* **81**(2): 260–273. doi:10.1016/j.yqres.2013.12.008

Rowan, A.V., Roberts, H.M., Jones, M.A., Duller, G.A.T., Covey-Crump, S.J., & Brocklehurst, S.H. (2012). Optically stimulated luminescence dating of glaciofluvial sediments on the Canterbury Plains, South Island, New Zealand. *Quaternary Geochronology* **8**: 10–22. doi:10.1016/j.quageo.2011.11.013

Shulmeister, J., Soons, J.M., Berger, G.W., Harper, M., Holt, S., Moar, N., Carter, J. A. (1999). Environmental and Sea-Level Changes on Banks Peninsula (Canterbury, New Zealand) through Three Glaciation–Interglaciation Cycles. *Palaeogeography, Palaeoclimatology, Palaeoecology **152***: 101–127. doi:10.1016/S0031-0182(99)00035-8

Sohbati, R., Borella, J., Murray, A., Quigley, M., Buylaert, J. (in review). Optical dating of loessic hillslope sediments constrains timing of prehistoric rockfalls, Christchurch, New Zealand. *Journal of Quaternary Science*.

Soons, J.M., Moar, N.T., Shulmeister, J., Wilson, H.D., Carter, J.A. (2002). Quaternary vegetation and climate changes on Banks Peninsula, South Island, New Zealand. *Global and Planetary Change* **33**: 301-314.

Stock, G. M., & Collins, B. D. (2014). Reducing Rockfall Risk in Yosemite National Park. *Eos, Transactions American Geophysical Union* **95**(29): 261–263. doi:10.1002/2014EO290002

Stoffel, M. (2006). A Review of Studies Dealing with Tree Rings and Rockfall Activity: The Role of Dendrogeomorphology in Natural Hazard Research. *Natural Hazards **39***(1): 51–70. doi:10.1007/s11069-005-2961-z

Stout, M., L. (1969). Radiocarbon Dating of Landslides in Southern California and Engineering Geology Implications. *Geological Society of America Special Papers* **123**: 167-180, doi: 10.1130/SPE123-p167

Stuiver, M., Polach, H.A. (1977). Reporting of ^{14}C Data. Radiocarbon **19**(3): 355-363.

Wilson, H.D. (1993). Bioclimatic zones and Banks Peninsula. *Canterbury Botanical Society Journal* **27**: 22-29.

Wilson, H.D. (2008). Natural history of Banks Peninsula. Canterbury University Press, Christchurch.

Wilson, H.D. (2013). Plant life on Banks Peninsula. Manuka Press, Cromwell.

Figure Captions

Figure 1) (a) Location map showing Rapaki study site and surrounding Port Hills and greater Banks Peninsula. (b) Rapaki study slope with prehistoric boulder and trench locations. Detailed logging was performed for PB2, PB3, PB4, and PB5 trenches. Mapped prehistoric boulders reflect boulder volume ≥0.1 m^3. (c) Photo showing prehistoric and modern (2011) boulders at the Rapaki study site. Prehistoric boulders are distinguishable from modern rockfall deposits because they are partially embedded in hillslope colluvium and are visible in pre-Canterbury earthquake sequence imagery. Surficial landslides (e.g. debris and mud flow) and extensive tunnel gulley formation and erosion are extensive on the modern deforested landscape. Locations for studied prehistoric boulders PB1-PB6 shown. Detailed trench logging was performed for PB2-PB5. (d) Photo of large modern boulder (~28 m3) detached from Mount Rapaki and emplaced in the Rapaki village during the 22 February 2011 earthquake. The boulder traveled through the center of the residential home located in background (center). Photo courtesy of D.J.A. Barrell, GNS Science.

Figure 2) (a) Photo of PB2 and surrounding hillslope sediment prior to exploratory trenching. (b) Photo of PB2 with pre-boulder (LC-1) and post-boulder (LC-2) emplacement hillslope sediments exposed. (c) Detailed stratigraphic log of PB2 and surrounding loess and loess-colluvium sediments. OSL sample locations and quartz and K-feldspar ages are shown. Phytolith samples (e.g. PS1-PS5) extracted from OSL locations. Mackey and Quigley (2014) ^{3}He CN surface exposure age for PB2 is shown.

Figure 3) (a) Photo of PB3 and surrounding hillslope sediment prior to exploratory trenching. (b) Photo of PB3 exploratory trench with pre-boulder and post-boulder emplacement hillslope sediments exposed. (c) Detailed stratigraphic log of PB3 and surrounding loess and loess-colluvium sediments. OSL (quartz=red; K-feldspar=blue) and radiocarbon sample locations and ages shown. Mackey and Quigley (2014) ^{3}He surface exposure age for PB3 also displayed.

Figure 4) (a) Photo of PB4 and surrounding hillslope sediment prior to exploratory trenching. (b) Photo of PB4 and exploratory trench with pre-boulder and post-boulder emplacement hillslope sediments exposed. Meter-stick shown for scale. (c) Stratigraphic log of PB4 and surrounding loess and loess-colluvium sediments. OSL sample locations and quartz and K-feldspar ages shown. Location and age (conventional and calibrated) for charcoal sample RapCH-06 displayed. Mackey and Quigley (2014) 3He surface exposure age for PB2 also displayed.

Figure 5) Photo of PB4 backside and exploratory trench with pre-boulder and post-boulder emplacement hillslope sediments exposed. Mackey and Quigley (2014) ^{3}He surface exposure age shown.

Figure 6) (a) Photo of PB5 and surrounding hillslope sediment prior to exploratory trenching. (b) Photo PB5 exploratory trench with pre-boulder and post-boulder emplacement hillslope sediments exposed. (c) Stratigraphic log of PB5 with surrounding

loess and loess-colluvium sediments. OSL sample locations and quartz and K-feldspar ages shown. Mackey and Quigley (2014) ^{3}He surface exposure age for PB5 displayed at top.

Figure 7) (a) Photo PB5 (front of boulder) exploratory trench with pre-boulder and post-boulder emplacement hillslope sediments exposed. (b) Stratigraphic log of PB5 with surrounding loess and loess-colluvium sediments. OSL sample location and quartz and K-feldspar ages shown. Mackey and Quigley (2014) 3He surface exposure age for PB5 displayed at top.

Figure 8) Summary of phytolith analysis from PB2 hillslope sediments. Luminescence sample depths and corresponding ages shown. Major climate phases (per Alloway et al., 2007) are displayed.

Figure 9) Examples of major phytolith morphologies extracted from Rapaki loess and loess-colluvium sediments. (A) Trapeziform polylobate: bone shaped (grass origin). (B) Conical short cell: spool shaped (grass origin). (C) Elongate long cell: rectangular shaped (grass origin). (D) Saddle short cell: circular with cut out (grass origin). (E) Cuniform bulliform cell: fan shaped (grass origin). (F) Polyhedral: hexagon shaped (tree/shrub origin). (G) Globular granular: spherical with surface ornamentation (tree/shrub origin). (H) Globular echinate: spherical with spiky ornamentation (New Zealand native nikau palm - Rhopalostylis sapida). Scale bar is 10 μm.

Figure 10) Quartz and K-feldspar luminescence age limits for the emplacement time of Rapaki prehistoric boulders PB2-PB5. Luminescence ages are compared with CN surface exposure ages from the top surface of the prehistoric boulders (Mackey and Quigley, 2014).

Table Captions

Table 1) Summary of Rapaki (NZ) sample name, boulder/trench location, burial depth, quartz OSL and K-feldspar pIRIR290 ages. Modified from Sobhati et al. (in review).

Table 2) Summary results from radiocarbon dating of charcoal within PB3 and PB4 loess-colluvium wedge sediments at the Rapaki study site.

Table 3) Summary for PB2 phytolith morphologies and relative percentages for grass, tree/shrub, and palm phytoliths.

Table 4) (a) Summary of trench stratigraphy and related field and laboratory measurements for PB2. (b) Summary of trench stratigraphy and related field and laboratory measurements for PB3. (c) Summary of trench stratigraphy and related field and laboratory measurements for PB4. (d) Summary of trench stratigraphy and related field and laboratory measurements for PB5.

Table 5) Summary of sediment accumulation rates, including sample name and ages used for rate determination, and measured stratigraphic thickness between samples.

Supplementary Figure Captions

Supplementary Figure 1) (a) Photo of PB1 prior to exploratory trenching. (b) Photo of PB1 with underlying sediments exposed. An OSL sample (shown) was retrieved within the in-situ loess and yields an OSL age of 29.3±2.5 ka (quartz) and 28.5±1.6 ka (K-feldspar). PB1 is located in an area of active tunnel gully erosion and deposition, and highlights the potential depositional complexities associated with prehistoric boulders on the Rapaki hillslope. Recent tunnel gully fill is found underlying PB1 and older loess collvium deposits.

Supplementary Figure 2) Photo of PB6 and adjacent (upslope) exploratory trench. Due to safety concerns, we were unable to expose the boulder base and identify the boulder emplacement surface. OSL sample location (ROSL-15; red circle) shown - sample not dated. PB6 is located within the axis of a drainage valley (see Figs. 1b and c) - a zone of active erosion and sediment (and potentially boulder) remobilization. Large volcanic clasts are observed to bottom of trench, indicating deposition by debris and mudflow and/or high velocity water flow. PB6 CN surface exposure age shown at top.

Supplementary Figure 3) Radiocarbon calibration report for charcoal sample RapCH-01.

Supplementary Figure 4) Radiocarbon calibration report for charcoal sample RapCH-03.

Supplementary Figure 5) Radiocarbon calibration report for charcoal sample RapCH-05.

Supplementary Figure 6) Radiocarbon calibration report for charcoal sample RapCH-06.

Supplementary Table Captions

Supplementary Table 1) Summary of grain size distribution for Rapaki hillslope sediments.

Sample Name	Boulder/Trench Location	Sample Depth	Quartz OSL age	K-feldspar $pIRIR_{290}$ age
		(cm)	(ka) ± se	(ka) ± se
ROSL-02	PB1	247	29.3±2.5	28.5±1.6
ROSL-03	PB2	70	2.8±0.3	2.46±0.15
ROSL-04	PB2	99	7.7±0.8	6.9±0.4
ROSL-05	PB2	116	12.5±1.1	10.8±0.6
ROSL-06	PB2	87	12.0±1.4	10.2±0.6
ROSL-07	PB2	171	27.2±3.0	21.8±1.4
ROSL-08	PB3	81	2.9±0.3	2.6±0.2
ROSL-09	PB3	170	5.8±0.5	6.5±0.4
ROSL-10	PB4	93	4.2±0.4	3.8±0.2
ROSL-11	PB4	120	10.3±1.0	10.4±0.7
ROSL-12	PB4	131	13.4±1.2	12.7±0.7
ROSL-13	PB5	31	1.7±0.2	1.94±0.14
ROSL-14	PB5	110	10.2±0.8	12.6±0.8

Table 1) Summary of Rapaki (NZ) sample name, boulder/trench location, burial depth, quartz OSL and K-feldspar pIRIR290 ages. Modified from Sobhati et al. (in review).

Sample ID	Boulder location	Exposure unit	NZA laboratory number	$\delta^{13}C$	Radiocarbon age (^{14}C yr B.P.)	Calibrated age 2σ (calendar yr A.D.)	Probability for each 2σ range (%)	Material
Rap-CH01	PB3	LC-2_R	56801	28.6±0.2	203±18	A.D. 1664-1698, **1724-1809**, 1870-1876	22.8, **70.4**, 1.0	Charcoal
Rap-CH03	PB3	LC-2_R	56802	29.1±0.2	197±17	A.D. 1666-1700, **1722-1810**, 1838-1845, 1867-1878, 1933-1938, 1946-1950	25.8, **63.8**, 1.3, 2.4, 0.6, 1.1	Charcoal
Rap-CH05	PB3	LC-2_R	56803	27.9±0.2	222±17	A.D. 1661-1680, **1732-1802**	15.8, **79.0**	Charcoal
Rap-CH06	PB4	LC-2_R	60079	26.9±0.2	162±22	A.D. 1667-1736, **1799-1950**	29.4, **65.7**	Charcoal

Note: NZA-Rafter Radiocarbon Laboratory; B.P. – before present

Table 2) Summary results from radiocarbon dating of charcoal within PB3 and PB4 loess-colluvium wedge sediments at the Rapaki study site.

Sample Name	Sediment Unit	Trapeziform polylobate *(grass)* %	Conical short cell *(grass)* %	Elongate long cell *(grass)* %	Saddle short cell *(grass)* %	Cuniform bulliform cell *(grass)* %	Polyhedral *(tree/shrub)* %	Globular granular *(tree/shrub)* %	Globular echinate *(palm)* %	Grasses (%)	Tree/ Shrub (%)	Palm (%)
PS-1	*In-situ* loess	6	2	13	1	9	6	35	28	32	40	28
PS-2	LC-1 (lower)	20	1	18	0	4	8	16	33	43	24	33
PS-3	LC-1 (upper)	12	0	23	2	1	10	11	41	37	22	41
PS-4	LC-2 (lower)	1	1	22	0	10	9	31	27	33	40	27
PS-5	LC-2 (upper)	4	0	16	1	1	7	3	68	22	10	68

Table 3) Summary for PB2 phytolith morphologies and relative percentages for grass, tree/shrub, and palm phytoliths.

Sediment Unit	Relative Timing	Colour	Texture	Relative Moisture	Sediment Strength	Bulk Density (cm^3)	Thickness (cm)	Structures
Loess	Predates PB2 emplacement	Light yellowish brown (2.5Y 6/4)	Silty loam comprised of ~30% sand, 60% silt, 10% clay, very little to no sediment derived from volcanic source rock	Dry	Hard	N/A	N/A	Massive, characteristic gammate structure with grey fissures/veins from desiccation/shrinkage, calcite-filled tubular root structures
LC-1	Predates PB2 emplacement	Light olive brown (2.5Y 5/3.5) with dark yellowish brown mottling (10YR 4/6)	Silty loam with minor gravel comprised of ~19% sand, 65% silt, 16% clay, slight but notable increase in coarser-grained sediment derived from proximal volcanic source rock, occasional pebble to cobble-sized clasts of basalt, maximum cobble diameter is ~23 cm)	Dry	Hard	1.93-2.04	58-84	Massive, abundant subvertical to vertical cracks with infilling calcite, well developed paleosol in upper 13-34 cm, paleosol contains clay coatings (worm castings), intense and pervasive mottling and abundant desiccation cracks, top of LC-1 marked by distinct unconformity
LC-2	Postdates PB2 emplacement	Grayish brown (10YR 5/2) with yellowish brown mottling (10YR 5/2) A horizon soil is very dark gray (2.5YR 3/1)	Silty loam with gravel to small boulder-sized fragments of volcanic rock (basalt), lower half of LC-2 comprised of ~13% gravel, 20% sand, 50% silt, 17% clay, upper half comprised of ~2% gravel, 26% sand, 59% silt, 13% clay (% gravel is conservative), significant increase in volcanic derived material, maximum diameter for volcanic rock is 18.87 cm	Damp to semi-moist	Soft to firm	1.59-1.92	110-128	Massive to very poorly layered, A-horizon soil (16-25 cm thick) is intensely altered and bioturbated, abundant small voids (dissolved roots, burrows)
IF-1	Postdates PB2 emplacement	Light gray (2.5Y 7/2) to light olive brown (2.5Y 5/4) with dark yellowish brown mottling (10YR 4/6)	Silty loam	Damp to dry	Stiff to very stiff	N/A	N/A	Laminations to thin layering (mm to cm scale) parallel to rear surface of PB2, minor rootlets and small mm-scale voids from burrowing
IF-2	Postdates PB2 emplacement	Very dark gray (2.5Y 3/1)	Silty loam	Damp to semi-moist	Soft to firm	N/A	N/A	No obvious layering, less oxidized than IF-1, small rootlets and mm-scale voids

Table 4a) Summary of trench stratigraphy and related field and laboratory measurements for PB2.

Sediment Unit	Relative Timing	Colour	Texture	Relative Moisture	Sediment Strength	Bulk Density (cm^3)	Thickness (cm)	Structures
Loess	Predates PB3 emplacement	Light yellowish brown (2.5Y 6/3) to light olive brown (2.5Y 5/4)	Silty loam comprised of ~36% sand, 51% silt, 13% clay, very little to no sediment derived from volcanic source rock	Dry	Hard	N/A	N/A	Massive, small vertical to subvertical desiccation cracks observed but not abundant, calcite filled tubular root structures, some mottling (iron oxidation)
LC-1	Predates PB3 emplacement	Grayish brown (2.5Y 5/2) to light olive brown (2.5Y 5/3) with yellowish brown mottling (10YR 5/8	Silty loam with minor gravel comprised of ~28% sand, 58% silt, 14% clay, slight but notable increase in coarser-grained sediment derived from proximal volcanic source rock, occasional pebble to cobble-sized clasts of basalt, maximum cobble diameter is ~8.8 cm	Dry	Hard	1.9-2.01	44-65	Massive, tiny mm-scale voids (e.g. burrows, dissolved roots), less well defined paleosol in upper 17-34 cm of LC-1, occasional old worm burrows with clay coatings and desiccation cracks observed, top of LC-1 is marked by unconformity
LC-2	Postdates PB2 emplacement	Brown to grayish brown (10YR 5/2) with brownish yellow (10YR 6/8) mottling	Silty loam with minor gravel, slight increase in coarse-grained sand and gravel, occasional pebbles/small cobbles of basalt, LC-2 sediment significantly less dense than underlying LC-1 sediment	Damp to semi-moist	Soft to firm	1.27 -1.59	24 LC-2 compara-tively thin	Massive to very poorly layered, abundant mottling, tiny rootlets pervasive
$LC\text{-}2_R$	Postdates PB2 emplacement	Grayish brown (2.5Y 5/2) to very dark gray (2.5Y 4/1) A horizon soil is very dark gray (2.5Y 3/1)	Silty loam comprised of ~24% sand, 64% silt, 12% clay with minor gravel, charcoal abundant, small fragments of charred brick/pottery	Dry to slightly damp	Soft	1.27	70	Moderately to poorly layered, abundant roots and other organic matter (e.g. wood, charcoal), charcoal primarily observed within the lower 30 cm of $LC\text{-}2_R$, no infill episodes observed adjacent to PB3

Table 4b) Summary of trench stratigraphy and related field and laboratory measurements for PB3.

Sediment Unit	Relative Timing	Color	Texture	Relative Moisture	Sediment Strength	Bulk Density (cm^3)	Thickness (cm)	Structures
Loess	Predates PB4 emplacement	Light yellowish brown (2.5Y 6/3) to light olive brown (2.5Y 5/3)	Sandy loam comprised of ~53% sand, 35% silt, 12% clay, we note increased sand % for PB4 loess	Dry	Hard	N/A	N/A	Massive, desiccation cracks infilled with dark brown translocated clay, infilled cracks are part of prismatic structure and taper (i.e. become thinner) with depth, cracks are vertical to subvertical and horizontal to subhorizontal, maximum width for desiccation cracks is ~3.5 cm, calcite-filled root structures, tiny rootlets
LC-1	Predates PB4 emplacement	Olive brown (2.5Y 4/3) with dark yellowish brown (10YR 4/6) mottling	Silty loam comprised of ~35% sand, 49% silt, 16% clay with minor gravel, observe increase in coarse-grained sand and gravel sized material derived from the volcanic source rock, several subangular to subrounded, pebble to small cobble-sized basalt clasts, maximum cobble diameter is ~11 cm.	Dry to damp	Hard	2.17	18-39	Massive, entirety of LC-1 has been affected by soil forming process, clay coatings with worm castings abundant, pervasive mottling, top of LC-1 is marked by a distinct unconformity
LC-2	Postdates PB4 emplacement	Grayish brown (10YR 5/2) to dark grayish brown (2.5YR 4/2) with dark yellowish brown (10YR 3/6) mottling	Silty loam comprised of ~24% sand, 57% silt, 19% clay with minor gravel, gravel-sized 'stones' (3-6 mm diameter) are commonly encountered within the predominantly silty matrix Upward grades into silty loam consisting of ~19% sand, 66% silt, 15% clay with minor gravel	Damp to semi-moist	Soft to firm	1.63-1.94	100	Massive to very poorly layered, abundant mottling, small rootlets pervasive, thin white lamination layer (~2-3 mm thick) is observed at depth of ~50 1-2 mm fragment of charcoal logged at depth of ~33 cm Upper 35-52 cm of LC-2 may be time equivalent PB3 LC-2_R sediments
IF-1	Postdates PB4 emplacement	Dark gray (2.5 YR 3/1)	Silty loam, similar in character to PB2 IF-2	Damp to semi-moist	Soft to firm	N/A	N/A	No obvious layering, small rootlets and mm-scale voids

Table 4c) Summary of trench stratigraphy and related field and laboratory measurements for PB4.

Sediment Unit	Relative Timing	Colour	Texture	Relative Moisture	Sediment Strength	Bulk Density (cm^3)	Thickness (cm)	Structures
Loess	Predates PB2 emplacement	Light yellowish brown (2.5YR 6/3) to light olive brown (2.5YR 5/4)	Silty loam comprised of ~39% sand, 50% silt, 11% clay	Dry	Hard	N/A	~100-200	Massive, desiccation cracks near top infilled with clay/silt, burrowing, calcite filled root structures
LC-1	Predates PB2 emplacement	Light yellowish brown (2.5YR 6/3) with yellowish brown mottling (10YR 4/6)	Silty loam comprised of ~26% sand, 62% silt, 12% clay; small increase (relative to in-situ loess) in volcanic derived subangular to subrounded, coarse-grained sand and gravel	Dry	Hard	1.83	29-44	Massive, subvertical to vertical desiccation cracks commonly filled with calcite, well developed paleosol with abundant mottling (iron oxidation), paleosol contains clay coated worm casts, top of paleosol marked by distinct unconformity
LC-2	Postdates PB2 emplacement	Grayish brown (10YR 5/2), within A-horizon very dark gray (2.5YR 3/1)	Silty loam with minor gravel comprised of (~32% sand, 55% silt, 13% clay); relative increase in coarse-grained sand and gravel A-horizon soil is silty loam comprised of ~31% sand, 58% silt, 11% clay	Dry to damp	Soft to firm	1.30	37-47 A-horizon is 17-34 cm	Massive to very poorly layered, A-horizon soil intensely altered and bioturbated, abundant small voids (dissolved roots, burrows)

Table 4d) Summary of trench stratigraphy and related field and laboratory measurements for PB5.

Boulder/ Trench	Unit	Sediment accumulation rate	Luminescence and radiocarbon samples used for rate determination	Time between bracketing samples	Measured stratigraphic thickness between samples
		(mm/a)		*(a)*	*(mm)*
PB2	LC-2	*Upper LC-2* 0.23 (Q) 0.27 (K)	ROSL-03; Existing ground surface (t=0)	2,800 (Q) 2,400 (K)	640
		Lower LC-2 0.07 (Q) 0.08 (K)	ROSL-04; ROSL-03	4,900 (Q) 4,500 (K)	360
	LC-1	N/A	N/A	N/A	N/A
	Loess	N/A	N/A	N/A	N/A
PB3	$LC\text{-}2_R$	2.13	RAP-CH01; Existing ground surface (t=0)	250*	532
	LC-2	0.05 (Q) 0.05 (K)	ROSL-08; RAP-CH01	2,650 (Q) 2,450 (K)	128
	LC-1	N/A	N/A	N/A	N/A
	Loess	N/A	N/A	N/A	N/A
PB4	$LC\text{-}2_R$	2.1	RAP-CH06	155*	358
	LC-2	0.22 (Q) 0.25 (K)	ROSL-10; Existing ground surface (t=0)	4,200 (Q) 3,700 (K)	926
	LC-1	0.04 (Q) 0.05 (K)	ROSL-12 & ROSL-11	3,200 (Q) 2,500 (K)	120
	Loess	N/A	N/A	N/A	N/A
PB5	LC-2	0.18 (Q) 0.16 (K)	ROSL-13 & Existing ground surface (t=0)	1,700 (Q) 1,900 (K)	304
	LC-1	N/A	N/A	N/A	N/A
	Loess	N/A	N/A	N/A	N/A

*ages from radiocarbon dating of charcoal samples; (Q)=from quartz luminescence ages, (K)=from K-feldspar luminescence ages

Table 5) Summary of sediment accumulation rates, including sample name and ages used for rate determination, and measured stratigraphic thickness between samples.

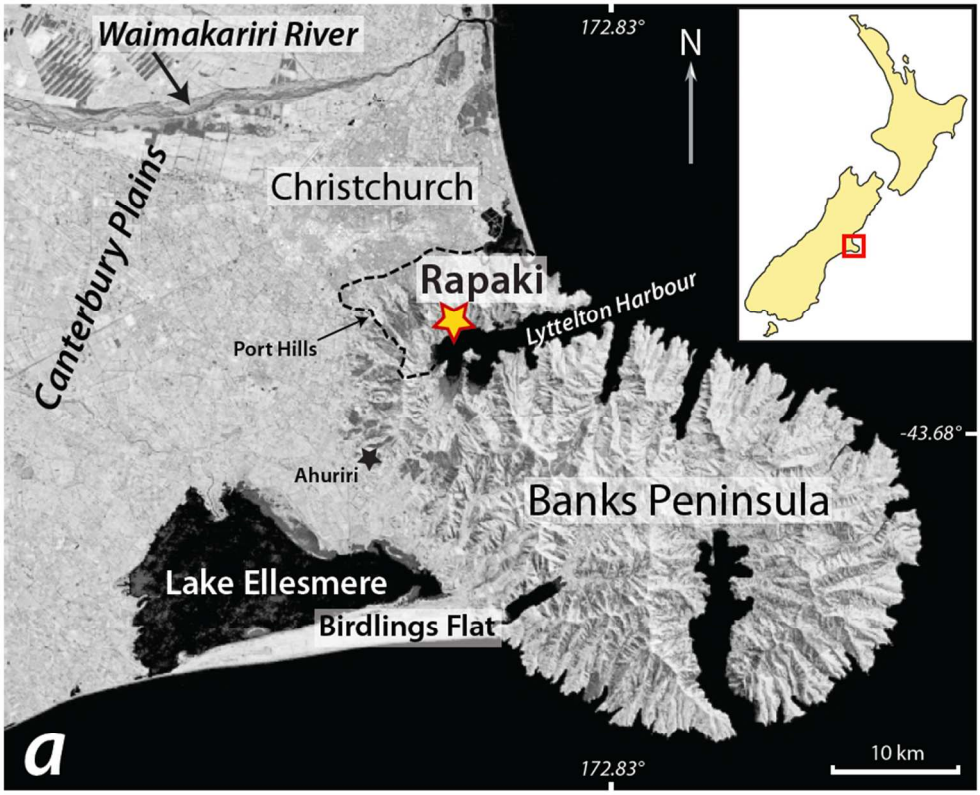

Figure 1a

Location map showing Rapaki study site and surrounding Port Hills and greater Banks Peninsula.
342x289mm (72 x 72 DPI)

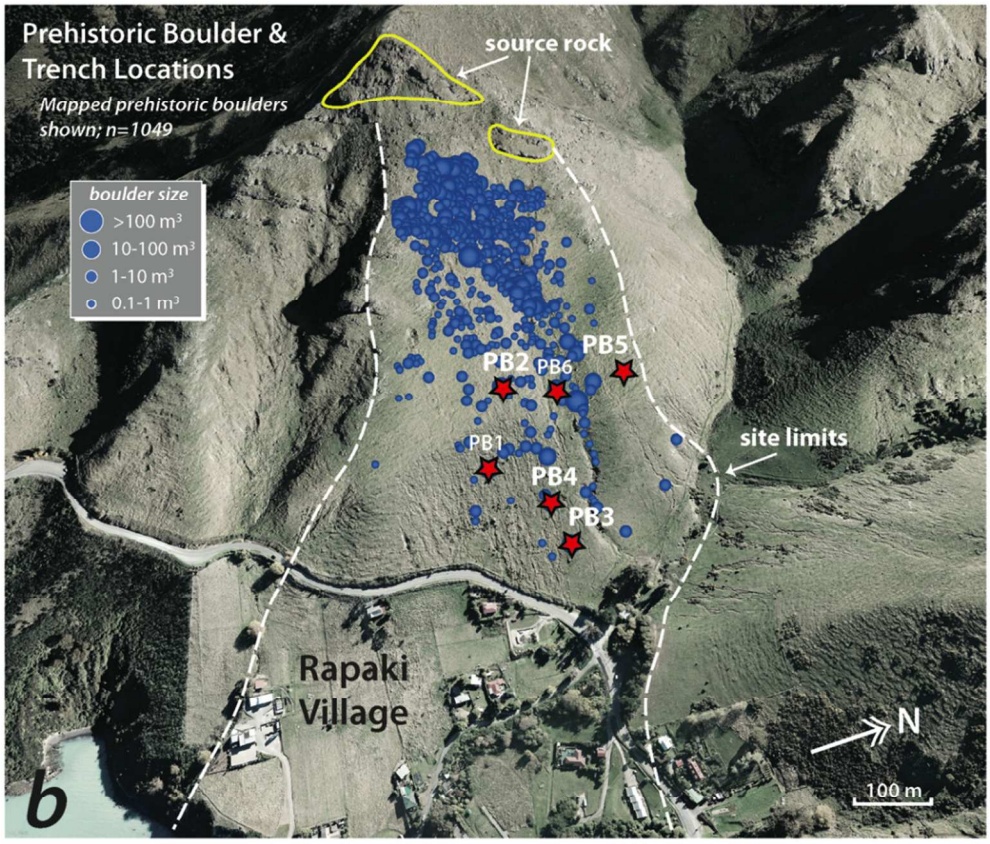

Figure 1b

Rapaki study slope with prehistoric boulder and trench locations. Detailed logging was performed for PB2, PB3, PB4, and PB5 trenches. Mapped prehistoric boulders reflect boulder volume ≥0.1 m3.
388x347mm (72 x 72 DPI)

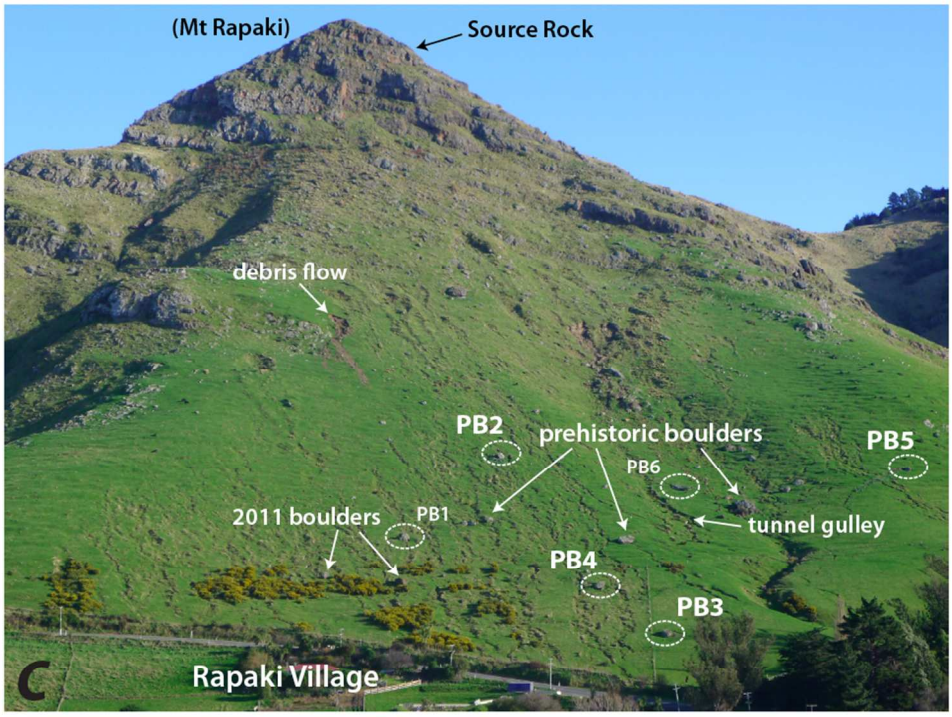

Figure 1c

Figure 1c) Photo showing prehistoric and modern (2011) boulders at the Rapaki study site. Prehistoric boulders are distinguishable from modern rockfall deposits because they are partially embedded in hillslope colluvium and are visible in pre-Canterbury earthquake sequence imagery. Surficial landslides (e.g. debris and mud flow) and extensive tunnel gulley formation and erosion are extensive on the modern deforested landscape. Locations for studied prehistoric boulders PB1-PB6 shown. Detailed trench logging was performed for PB2-PB5.
359x286mm (72 x 72 DPI)

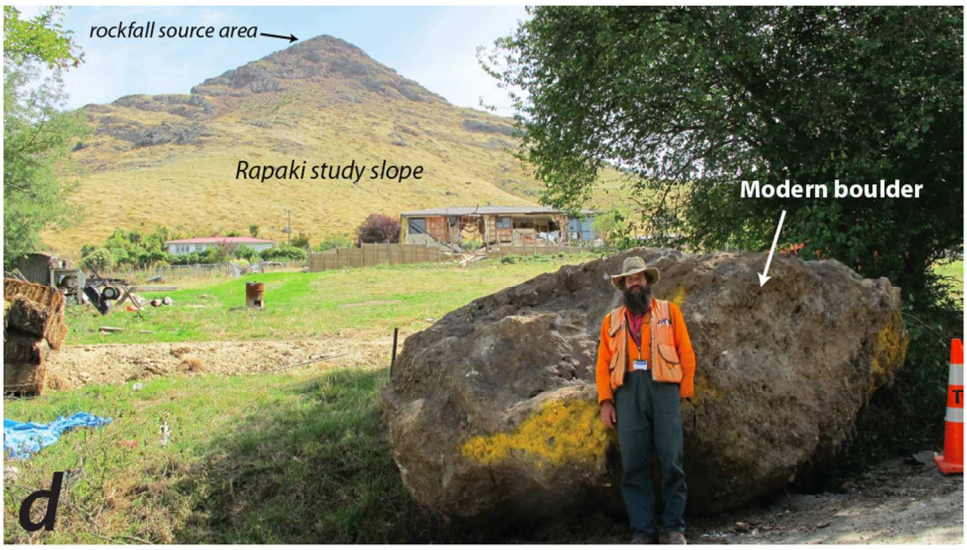

Figure 1d

Figure 1d) Photo of large modern boulder (~28 m3) detached from Mount Rapaki and emplaced in the Rapaki village during the 22 February 2011 earthquake. The boulder traveled through the center of the residential home located in background (center). Photo courtesy of D.J.A. Barrell, GNS Science.
357x225mm (72 x 72 DPI)

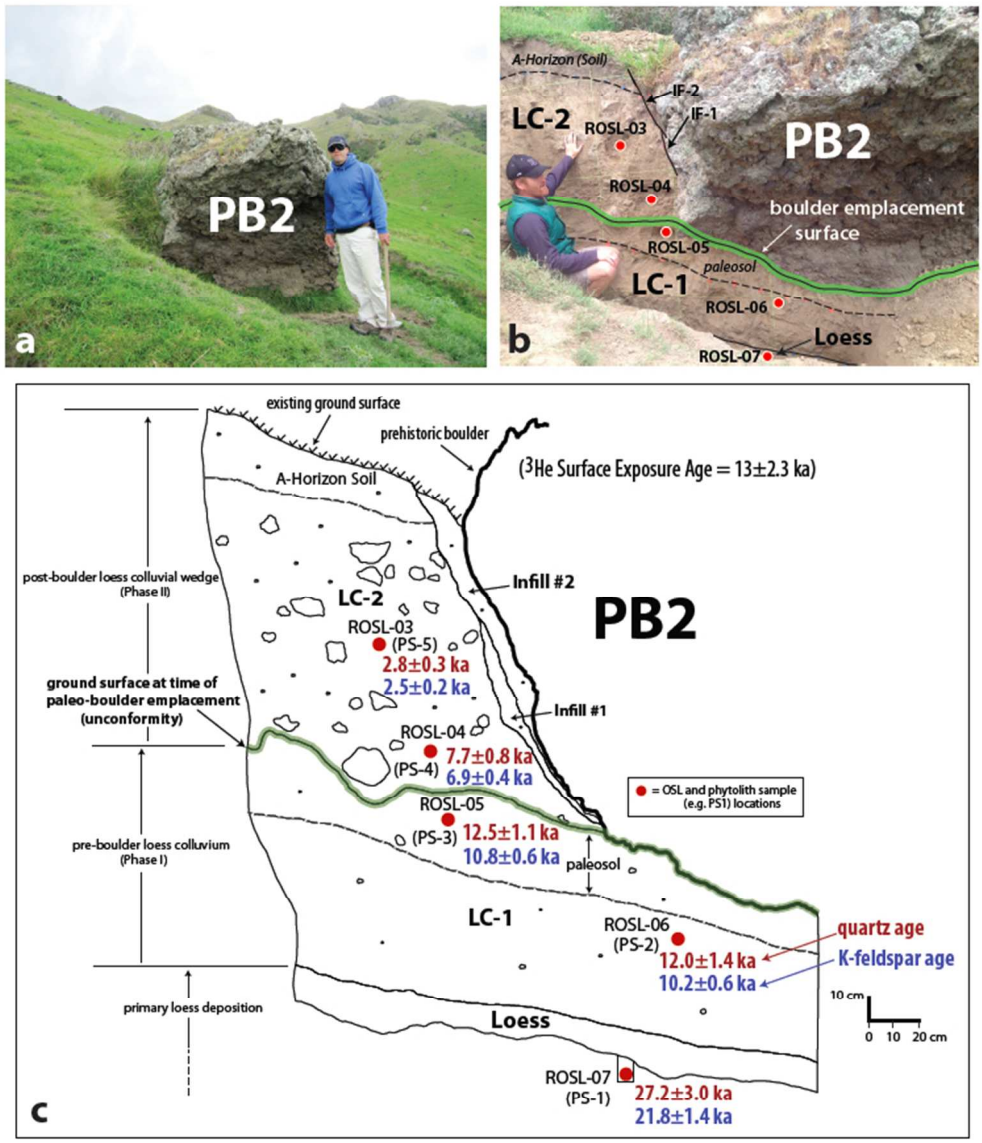

Figure 2a,b,c

Figure 2) (a) Photo of PB2 and surrounding hillslope sediment prior to exploratory trenching. (b) Photo of PB2 with pre-boulder (LC-1) and post-boulder (LC-2) emplacement hillslope sediments exposed. (c) Detailed stratigraphic log of PB2 and surrounding loess and loess-colluvium sediments. OSL sample locations and quartz and K-feldspar ages are shown. Phytolith samples (e.g. PS1-PS5) extracted from OSL locations. Mackey and Quigley (2014) 3He CN surface exposure age for PB2 is shown.
264x322mm (72 x 72 DPI)

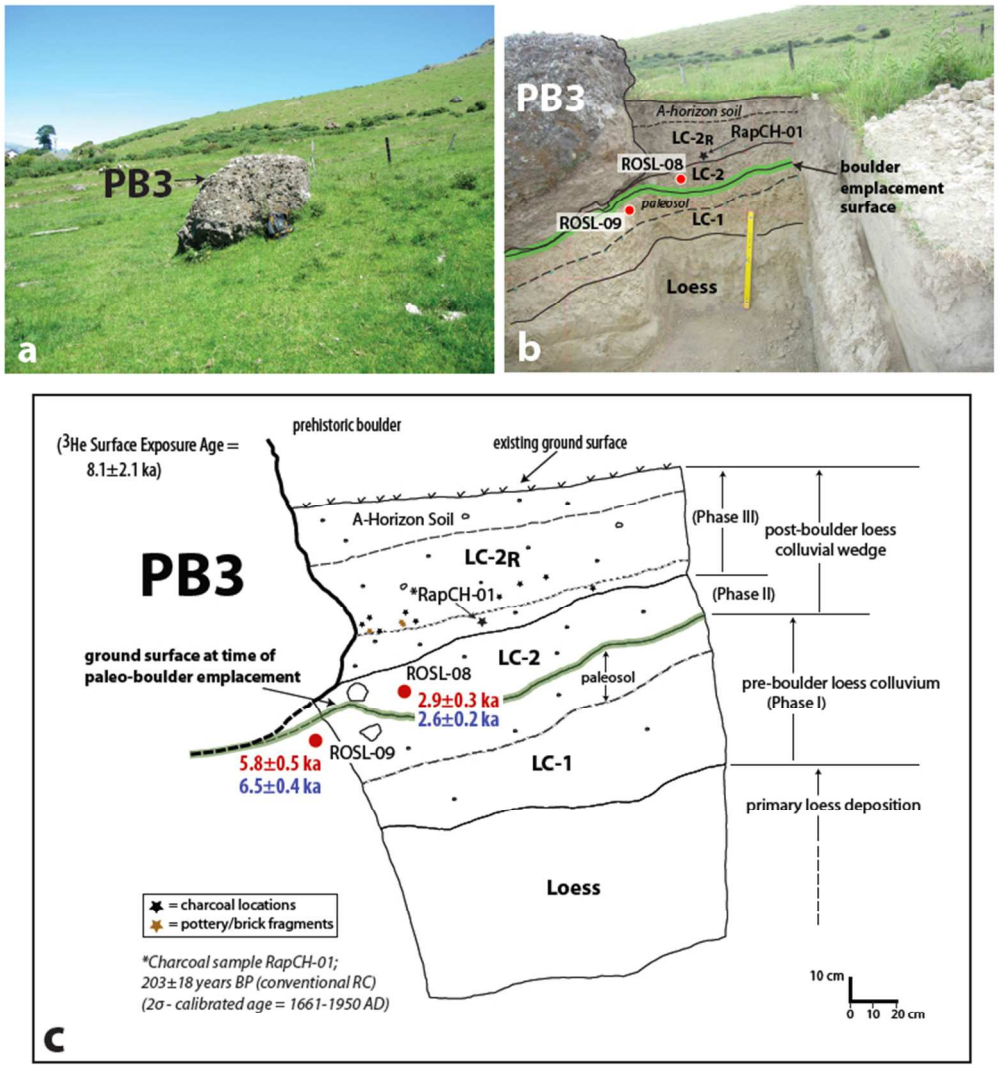

Figure 3a,b,c

Figure 3) (a) Photo of PB3 and surrounding hillslope sediment prior to exploratory trenching. (b) Photo of PB3 exploratory trench with pre-boulder and post-boulder emplacement hillslope sediments exposed. (c) Detailed stratigraphic log of PB3 and surrounding loess and loess-colluvium sediments. OSL (quartz=red; K-feldspar=blue) and radiocarbon sample locations and ages shown. Mackey and Quigley (2014) 3He surface exposure age for PB3 also displayed.
284x316mm (72 x 72 DPI)

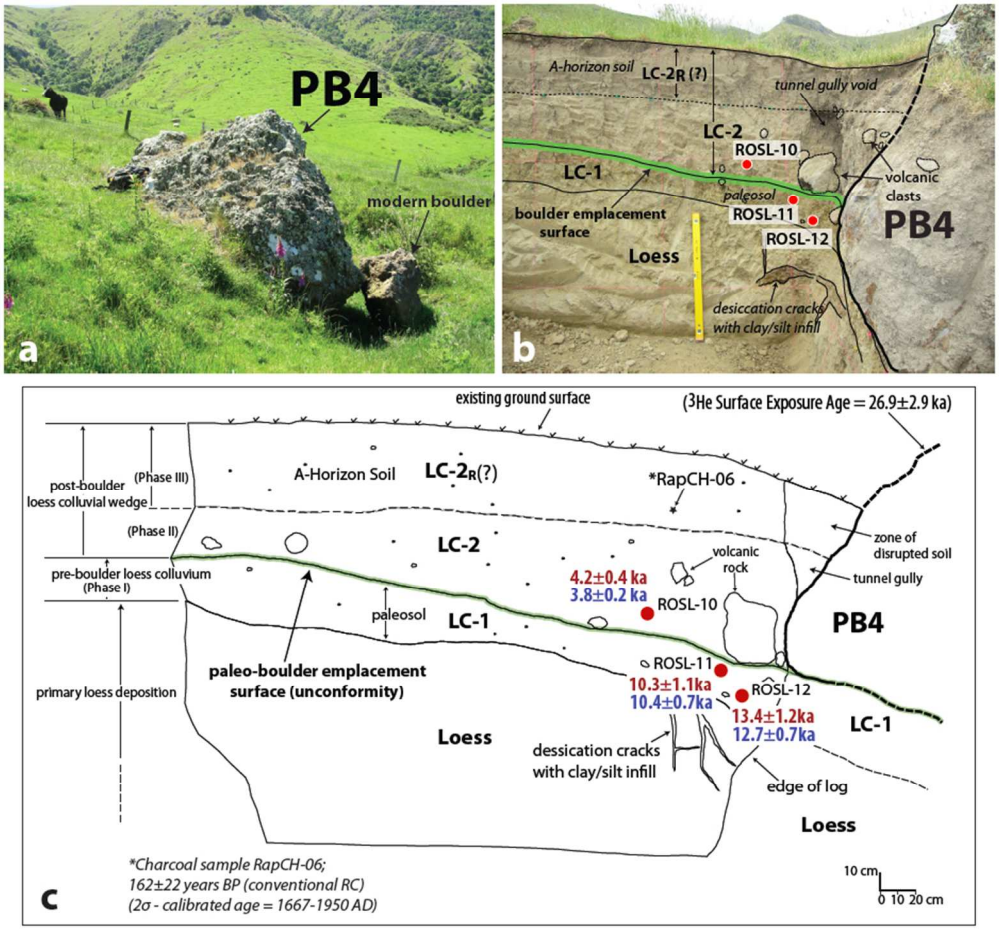

Figure 4a,b,c

Figure 4) (a) Photo of PB4 and surrounding hillslope sediment prior to exploratory trenching. (b) Photo of PB4 and exploratory trench with pre-boulder and post-boulder emplacement hillslope sediments exposed. Meter-stick shown for scale. (c) Stratigraphic log of PB4 and surrounding loess and loess-colluvium sediments. OSL sample locations and quartz and K-feldspar ages shown. Location and age (conventional and calibrated) for charcoal sample RapCH-06 displayed. Mackey and Quigley (2014) 3He surface exposure age for PB2 also displayed.
331x324mm (72 x 72 DPI)

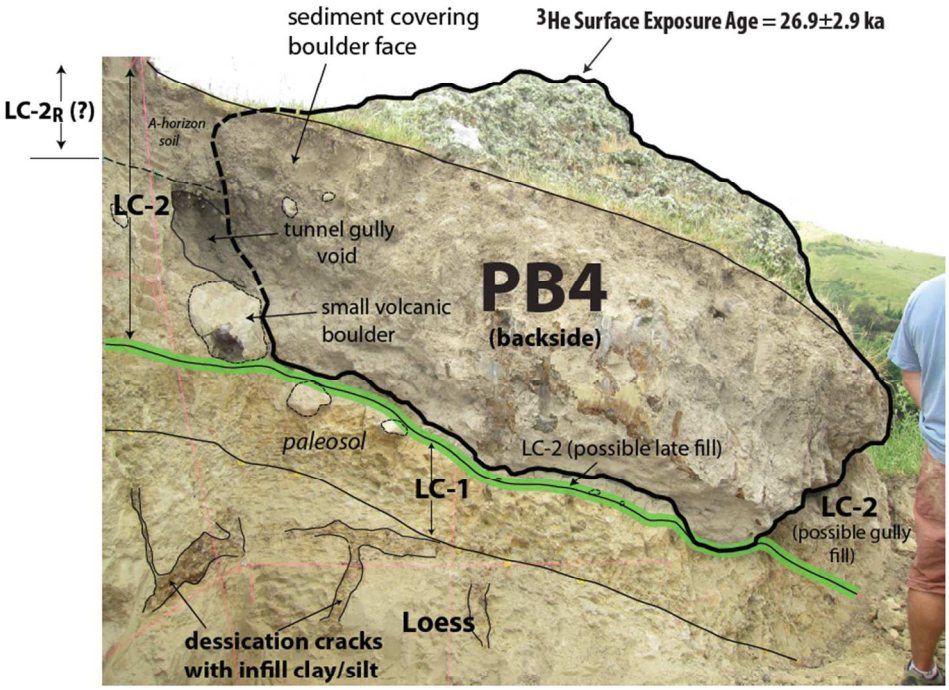

Figure 5

Figure 5) Photo of PB4 backside and exploratory trench with pre-boulder and post-boulder emplacement hillslope sediments exposed. Mackey and Quigley (2014) 3He surface exposure age shown.
348x275mm (72 x 72 DPI)

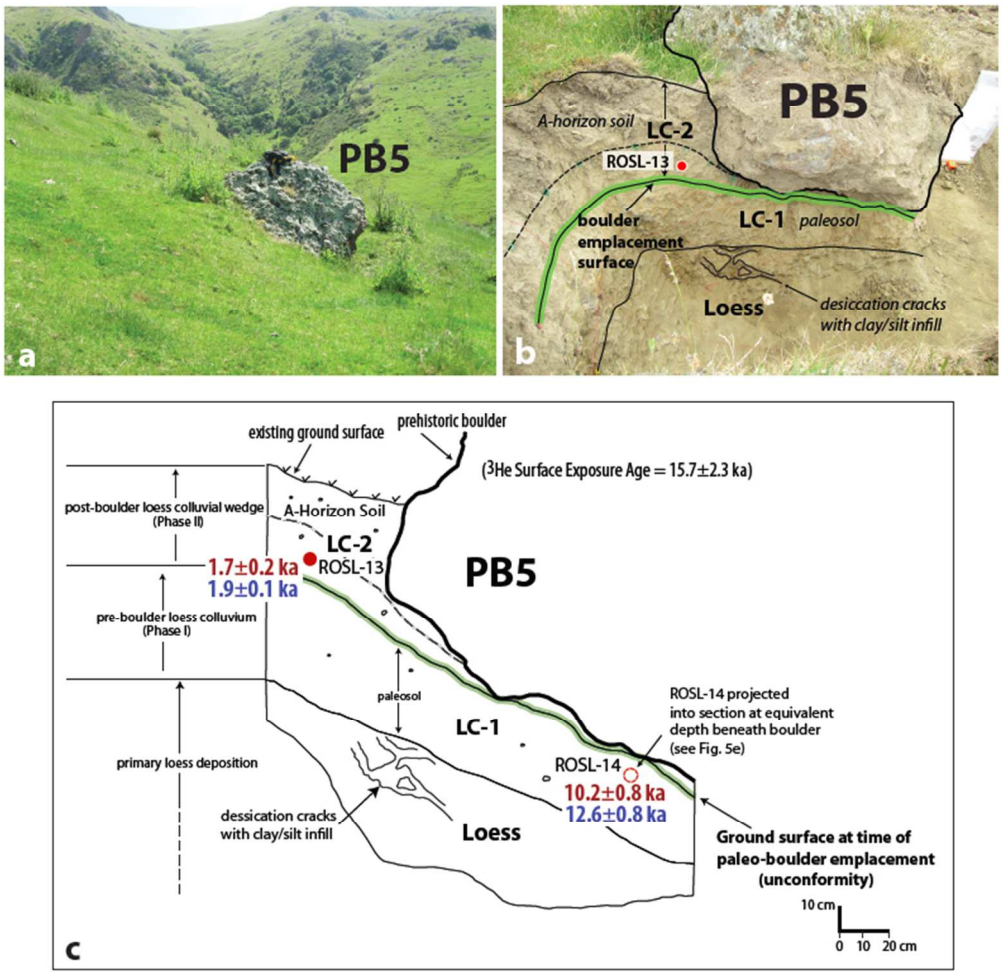

Figure 6a,b,c

Figure 6) (a) Photo of PB5 and surrounding hillslope sediment prior to exploratory trenching. (b) Photo PB5 exploratory trench with pre-boulder and post-boulder emplacement hillslope sediments exposed. (c) Stratigraphic log of PB5 with surrounding loess and loess-colluvium sediments. OSL sample locations and quartz and K-feldspar ages shown. Mackey and Quigley (2014) 3He surface exposure age for PB5 displayed at top.
279x285mm (72 x 72 DPI)

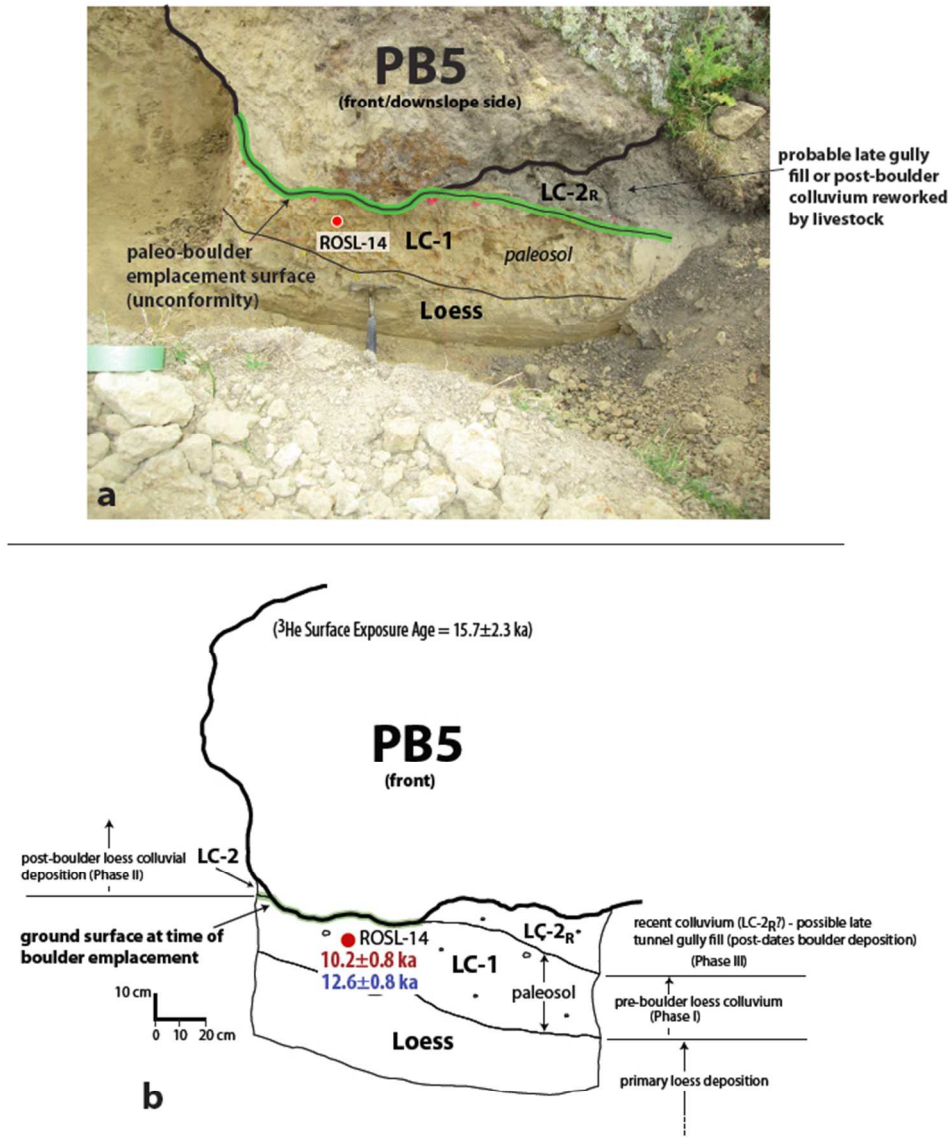

Figure 7a,b

Figure 7) (a) Photo PB5 (front of boulder) exploratory trench with pre-boulder and post-boulder emplacement hillslope sediments exposed. (b) Stratigraphic log of PB5 with surrounding loess and loess-colluvium sediments. OSL sample location and quartz and K-feldspar ages shown. Mackey and Quigley (2014) 3He surface exposure age for PB5 displayed at top.
259x319mm (72 x 72 DPI)

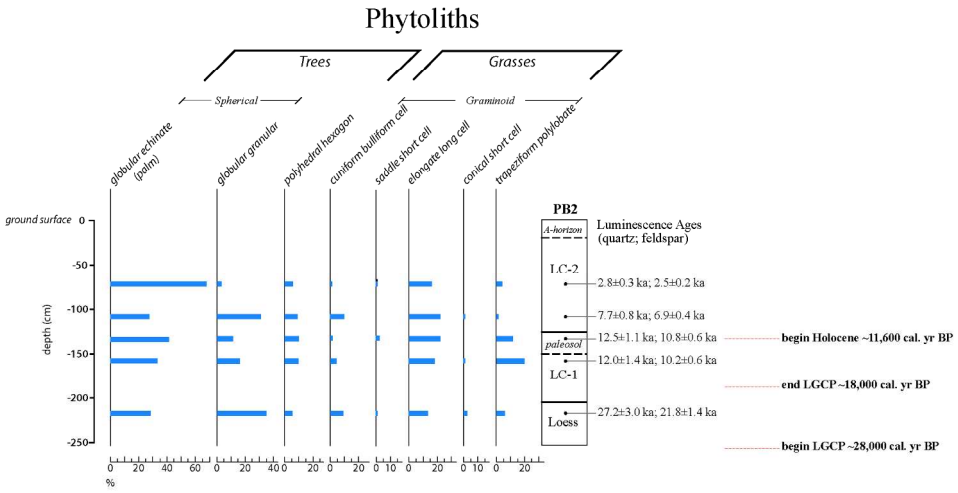

Figure 8

Figure 8) Summary of phytolith analysis from PB2 hillslope sediments. Luminescence sample depths and corresponding ages shown. Major climate phases (per Alloway et al., 2007) are displayed.
297x210mm (200 x 200 DPI)

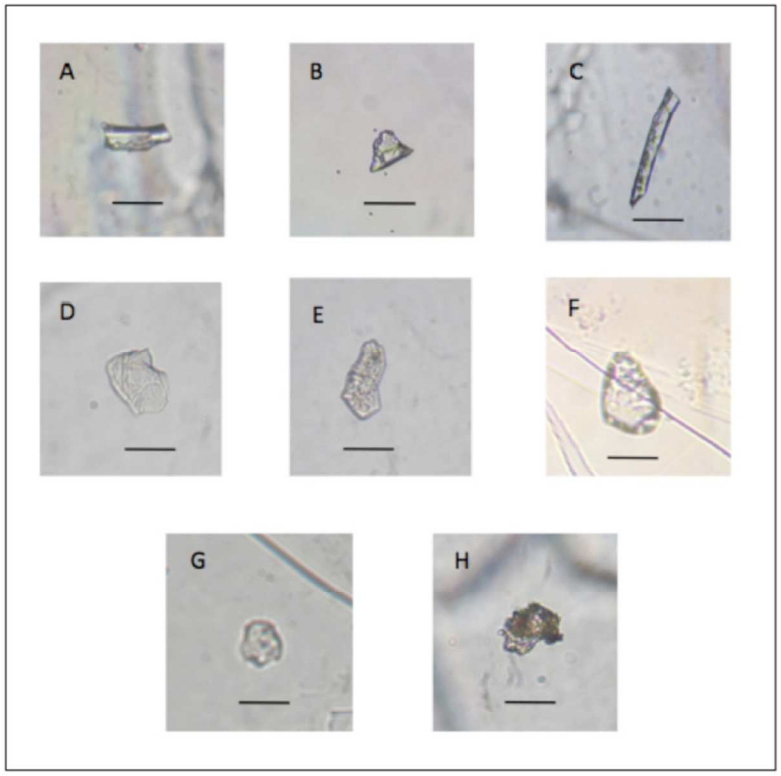

Figure 9

Figure 9) Examples of major phytolith morphologies extracted from Rapaki loess and loess-colluvium sediments. (A) Trapeziform polylobate: bone shaped (grass origin). (B) Conical short cell: spool shaped (grass origin). (C) Elongate long cell: rectangular shaped (grass origin). (D) Saddle short cell: circular with cut out (grass origin). (E) Cuniform bulliform cell: fan shaped (grass origin). (F) Polyhedral: hexagon shaped (tree/shrub origin). (G) Globular granular: spherical with surface ornamentation (tree/shrub origin). (H) Globular echinate: spherical with spiky ornamentation (New Zealand native nikau palm - Rhopalostylis sapida). Scale bar is 10 μm.
210x297mm (101 x 101 DPI)

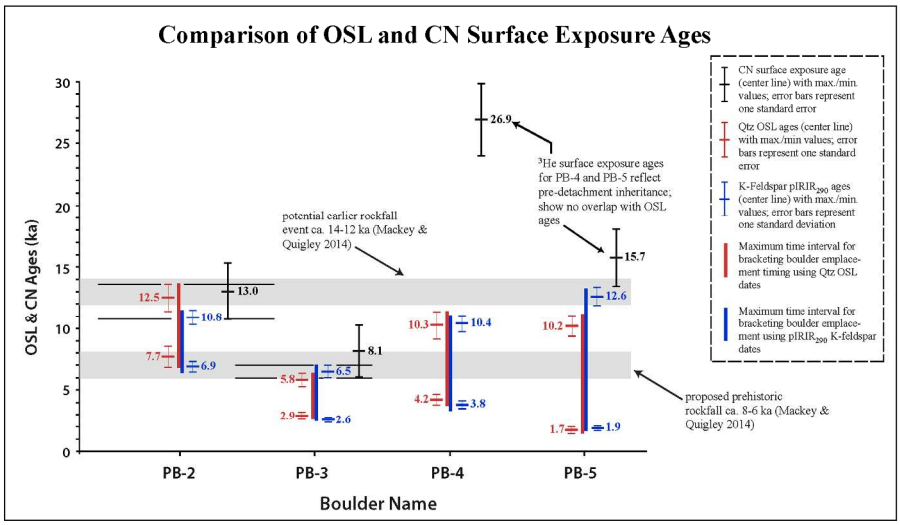

Figure 10

Figure 10) Quartz and K-feldspar luminescence age limits for the emplacement time of Rapaki prehistoric boulders PB2-PB5. Luminescence ages are compared with CN surface exposure ages from the top surface of the prehistoric boulders (Mackey and Quigley, 2014).
297x210mm (200 x 200 DPI)